Lithos xxx (xxxx) xxx

Contents lists available at ScienceDirect

Lithos

journal homepage: www.elsevier.com/locate/lithos

Research Article

Geochronology and geochemistry of the Xiaoqinling Taihua Complex in the southern Trans-North China Orogen: Implications for magmatism during the early Paleoproterozoic global tectono-magmatic shutdown

Xue Wang [a,b,c], Xiao-Long Huang [a,b,d,*], Fan Yang [a,b,d]

[a] State Key Laboratory of Isotope Geochemistry, Guangzhou Institute of Geochemistry, Chinese Academy of Sciences, Guangzhou 510640, China
[b] CAS Center for Excellence in Deep Earth Science, Guangzhou 510640, China
[c] College of Earth Science and Engineering, Shandong University of Science and Technology, Qingdao, Shandong 266590, China
[d] Southern Marine Science and Engineering Guangdong Laboratory (Guangzhou), Guangzhou 511458, China

ARTICLE INFO

Article history:
Received 21 July 2020
Received in revised form 13 May 2021
Accepted 19 May 2021
Available online xxxx

Keywords:
Orogenic collapse
Recycled materials
Early Paleoproterozoic
Global tectono-magmatic shutdown
Taihua Complex
Trans-North China Orogen

ABSTRACT

The Taihua Complex in the Xiaoqinling area of the southern Trans-North China Orogen (TNCO) records extensive magmatism during the early Paleoproterozoic. This contrasts with the tectono-magmatic quiescence recorded globally at this time. Based on zircon U−Pb geochronological and whole-rock geochemical data, the 2.36–2.30 Ga granitic gneisses in the Taihua Complex can be subdivided into three groups. Group-1 gneisses (2.36–2.33 Ga), mainly in the Dumutai area, are high-K_2O granitoid rocks, which record the earliest magmatism. These rocks have fractionated rare earth elements (REE) patterns, marked negative Eu−Sr anomalies, and variable whole-rock $\varepsilon_{Nd}(t)$ (−1.67 to +2.41) and $\varepsilon_{Hf}(t)$ values (−0.89 to +3.41), and were likely derived by partial melting of a mixture of pre-existing tonalite–trondhjemite–granodiorite (TTG) and K-rich rocks with residual plagioclase in the source at high-temperature and low-pressure conditions. Group-2 gneisses (2.33–2.31 Ga), mainly in the Jialu and Xitongyu areas, are granitoid rocks that formed after the Group-1 gneisses. These rocks have less fractionated REE patterns, low La/Yb and Sr/Y ratios, and slightly positive to negative whole-rock $\varepsilon_{Nd}(t)$ (−3.91 to +2.00) and $\varepsilon_{Hf}(t)$ values (−7.99 to +0.87), which resulted from high-degree partial melting of ancient crust in an extensional setting. Group-3 gneisses (~2.30 Ga) are TTG rocks from the Bayuan area, which represent the youngest magmatism. These rocks have high La/Yb and Sr/Y ratios, high MgO, Cr, and Ni contents, and negative whole-rock $\varepsilon_{Nd}(t)$ (−1.71 to −1.67) and $\varepsilon_{Hf}(t)$ values (−0.57 to −0.10), which indicate derivation by partial melting of delaminated lower crust and interaction with mantle materials. Samples from all groups have variable zircon $\varepsilon_{Hf}(t_{7/6})$ (−6.38 to +7.70) and $\delta^{18}O$ values (3.97‰ − 6.79‰), indicative of a heterogeneous magmatic source. Most zircons have slightly positive to negative $\varepsilon_{Hf}(t_{7/6})$ values, indicating significant reworking of ancient crustal materials and limited crustal growth during this period. The age, geochemistry, and petrogenesis of the studied granitoid rocks record orogenic collapse and a transition from post-collisional extension to crustal delamination in the early Paleoproterozoic. This followed late Archean subduction–collision–accretion processes in the southern NCC.

1. Introduction

The global distribution of U−Pb ages for subduction-related granitoids and detrital zircons indicates a widespread reduction in magmatic activity on Earth at 2.45–2.20 Ga, which is considered to represent a global magmatic and tectonic shutdown or slowdown (Condie, O'Neill, and Aster, 2009; Partin et al., 2014; Spencer, Murphy, Kirkland, Liu, and Mitchell, 2018). However, there was some magmatic activity during this period, such as mafic dike swarms in the Dharwar, Zimbabwe, Yilgarn, West Greenland, and Karelian cratons, the Fennoscandian Shield, and North America (Partin et al., 2014; Spencer, Murphy, Kirkland, Liu, and Mitchell, 2018 and references therein). These mafic igneous rocks were related to large igneous province events, mantle plumes, and break-up of the Kenorland supercontinent that formed in the late Archean (Eriksson and Condie, 2014; Partin et al., 2014, and references therein). Coeval silicic magmatism was relatively scarce, but includes tonalite–trondhjemite–granodiorite (TTG) suites in the Sãn Francisco, Amazonian (Brazil), West African, and North China cratons, and some calc-alkaline granitoids in the Qaidam Basin, Yangtze Block, Quanji Massif, and Arrowsmith Orogenic Belt of the Western Churchill Craton (e.g, Cui et al., 2019; Gong et al., 2014; Gong, He, Wang, Chen, and Kusky, 2019; He et al., 2018; Seixas, David, and Stevenson, 2012;

* Corresponding author at: State Key Laboratory of Isotope Geochemistry, Guangzhou Institute of Geochemistry, Chinese Academy of Sciences, Guangzhou 510640, China.
E-mail address: xlhuang@gig.ac.cn (X.-L. Huang).

https://doi.org/10.1016/j.lithos.2021.106248
0024-4937/

Teixeira et al., 2015; Yu, Fu, Wang, Li, and Guo, 2017; Zhao et al., 2008). The TTG suites are thought to have formed in a subduction-related arc setting, whereas the other granitoids were associated with *syn*- or post-collisional extension. The presence of these mafic and silicic rocks appears to contradict the model of a global tectono-magmatic shutdown.

The North China Craton (NCC; Fig. 1a) is the largest and oldest cratonic block in China (ca. 3.8 Ga; Liu, Nutman, Compston, Wu, and Shen, 1992; Song, Nutman, Liu, and Wu, 1996), and consists of Archean to Paleoproterozoic basement (Zhao, Sun, Wilde, and Li, 2005; Zhao and Zhai, 2013). Notably, early Paleoproterozoic magmatic activity in the NCC occurred during the global tectono-magmatic shutdown. Rocks formed during this period have been recognized in the Bayanwulashan Complex of the Alxa Block, the Daqingshan area of the Khondalite Belt, and the Lüliang, Zhongtiao, and Taihua complexes of the Trans-North China Orogen (TNCO) (Dan, Li, Guo, Liu, and Wang, 2012; Diwu, Sun, Zhao, and Lai, 2014; Dong et al., 2009; Huang, Wilde, Yang, and Zhong, 2012; Huang, Wilde, and Zhong, 2013; Yuan, Zhang, Yang, Lu, and Chen, 2017; Zhao et al., 2008). The Bayanwulashan mafic igneous rocks are geochemically similar to those formed in a continental rift, whereas the rocks from the TNCO formed in various tectonic settings: Intra-continental rifts, subduction zones, and integrated rift–subduction–collisional settings (e.g., Dan, Li, Guo, Liu, and Wang, 2012; Trap, Faure, Lin, and Monié, 2007; Yuan, Zhang, Yang, Lu, and Chen, 2017; Zhai and Liu, 2003; Zhao et al., 2008). The petrogenesis of these rocks and their geodynamic settings are key in understanding the early Paleoproterozoic tectonic evolution of the NCC.

The Taihua Complex in the Xiaoqinling area is the largest outcrop of Precambrian basement in the southern TNCO, and records early Neoarchean to late Paleoproterozoic magmatism, including extensive silicic magmatism at ca. 2.3 Ga (e.g., Diwu, Sun, Zhao, and Lai, 2014; Huang, Wilde, and Zhong, 2013; Jia et al., 2016, 2019; Wang et al.,

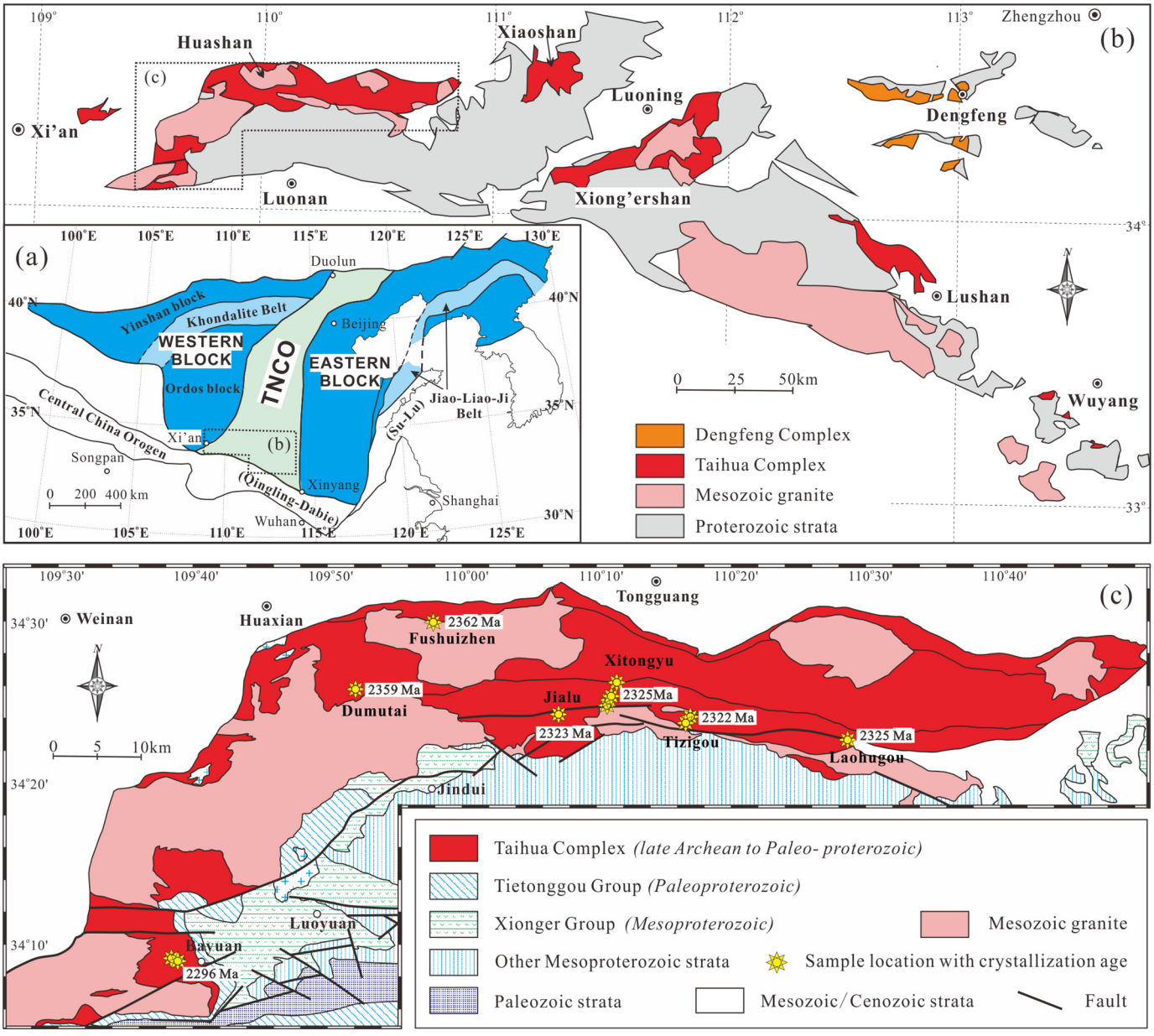

Fig. 1. (a) Tectonic framework of the North China Craton (after Zhao, Sun, Wilde, and Li, 2005); (b) sketch map of the early Precambrian terranes in the southern Trans-North China Orogen (after Diwu, Sun, Zhao, and Lai, 2014); (c) geological map of the Taihua Complex in the Xiaoqinling area, showing sample locations (after Huang, Wilde, and Zhong, 2013).

2012, 2017a; Wang, Wang, Chen, Lu, and Wu, 2014; Yu, Liu, Li, Chen, and Dai, 2013). As such, the Xiaoqinling area is an ideal site for investigating the early Paleoproterozoic tectonic evolution of the NCC. However, the petrogenesis of igneous rocks and related tectonic processes in this region are controversial because these ca. 2.3 Ga rocks show diverse petrological and geochemical characteristics. For example, abundant granites in the Xiaoqinling area have been proposed to have formed in an extensional setting (Jia et al., 2019), whereas the TTGs were derived by partial melting of thickened lower crust with residual garnet and amphibole, which possibly occurred in an orogenic setting (Huang, Wilde, and Zhong, 2013). Therefore, the key issue is whether these ca. 2.3 Ga rocks were formed in a simple tectonic event.

In this paper, we present whole-rock geochemical and Nd—Hf isotope data, and in situ zircon U—Pb ages and Hf—O isotopic data for granitoid gneisses from the Taihua Complex. We use these data to investigate the petrogenesis and source characteristics of these rocks, and to constrain the tectonic evolution of the southern NCC during the early Paleoproterozoic global tectono-magmatic shutdown.

2. Geological setting and sample descriptions

The NCC is tectonically bounded by the Central Asian Orogenic Belt (CAOB) to the north, the Qinling–Dabie orogenic belt to the south, the Qilian Orogen to the west and the Sulu HP–UHP metamorphic belt to the east. It consists of two distinct blocks (i.e., the Eastern and Western blocks) that were amalgamated in the Paleoproterozoic (ca. 1.85 Ga) to form the N—S trending TNCO (Fig. 1a; Zhao, Sun, Wilde, and Li, 2005). The Western Block formed by amalgamation of the Yinshan and Ordos blocks along the E–W trending Khondalite Belt at ca. 1.95 Ga (Fig. 1a; Zhao, Sun, Wilde, and Li, 2005), whereas the Eastern Block underwent a Paleoproterozoic (2.2–1.9 Ga) rifting event and subsequent subduction-collision processes, forming the Paleoproterozoic Jiao–Liao–Ji Belt (1.90 Ga, Fig. 1a, Li and Zhao, 2007, Tam et al., 2011, Zhao and Zhai, 2013). Archean basement rocks (3.8–2.5 Ga) are widely exposed in the Eastern Block.

The Taihua Complex, usually termed as the Taihua Group in the traditional Chinese literature, is exposed in an E–W-trending belt from the Xiaoqinling, Xiaoshan, Xiong'er, Lushan, to Wuyang areas in the southern TNCO (Fig. 1b). The Taihua Complex in the Xiaoqinling area is the largest outcrop of Precambrian basement in the southern segment of the TNCO (Fig. 1c), which was further subdivided into the Lower and Upper Taihua Groups according to rock types (Guan, 1996; Qi, 1992). The Upper Taihua Group consists of quartzite, metapelitic gneiss and schist, marble and iron formation, whereas the Lower Taihua "Group" consists of amphibolite and intermediate to felsic gneisses, with minor granulites (Qi, 1992). Collectively, the Taihua Complex in the Xiaoqinling area is a meta-volcanic sedimentary sequence that mainly comprises Mesoarchean–Paleoproterozoic TTG gneisses, granitic rocks, and minor amphibolites, which typically experienced high amphibolite- to granulite-facies metamorphism in the Paleoproterozoic (1.9–1.8 Ga, Jia et al., 2016; Wang et al., 2012; Wang, Wang, Chen, Lu, and Wu, 2014). The Taihua Complex in the Xiaoqinling area is unconformably overlain by Quaternary sediments and the Paleoproterozoic Tietonggou Formation or Mesoproterozoic Xiong'er Group (Fig. 1c; Guan, 1996; Huang, Wilde, and Zhong, 2013; Jia et al., 2016; Shen, 1986).

In this study, gneiss samples of the Taihua Complex were collected from the Jialu, Xitongyu, Fushuizhen, Tizigou, Laohugou, and Bayuan areas (Fig. 1c). Most of the gneisses are banded with parallel light and dark layers (Fig. 2a) that have different mineral proportions. The gneisses contain plagioclase (30%–50%), biotite (10%–25%), amphibole (10%–20%) and quartz (10%–15%) (Fig. 2b), and some contain K-feldspar (<10%), suggesting an amphibolite-facies metamorphism. The gneissic fabrics are defined by the parallel alignment of biotite and/or amphibole (Fig. 2b). Some gneiss samples from Bayuan are weakly layered (Fig. 2c), and consist of plagioclase (30%–40%), amphibole (10%–30%), biotite (10%–20%), quartz (10%–20%), and minor garnet (Fig. 2d). Titanite, magnetite, apatite, and zircon are common accessory minerals (<1%) in all samples.

3. Analytical methods

All analyses were carried out at the State Key Laboratory of Isotope Geochemistry, Guangzhou Institute of Geochemistry, Chinese Academy of Sciences (GIG-CAS). Analytical procedure and conditions are principally similar to those described by Wang, Huang, Yang, and Luo (2017b); Wang, Huang, and Yang (2019).

Whole-rock major element oxides were determined using a Rigaku RIX 2000 X-ray fluorescence (XRF) spectrometer, and analytical uncertainties are mostly between 1% and 5%. Trace elements were analyzed by Perkin-Elmer Sciex ELAN 6000 inductively coupled plasma-mass spectrometry (ICP-MS) after acid digestion of samples in high-pressure Teflon bombs. The US Geological Survey and Chinese National Standards SARM-4, SY-4, BHVO-2, AGV-2, GSD-9, GSR-1, GSR-2, GSR-3 and GSR-10 were used for calibration. Analytical precision of REE and other incompatible elements is typical 1–5%.

Whole-rock Nd—Hf isotopic analyses were performed on a Neptune Plus multi-collector ICP-MS (MC-ICP-MS). All chemical preparations were performed on the specially designed class-100 work benches inside a class-1000 clean laboratory. The samples for Nd isotopic analysis were dissolved by the acid mixtures of HNO_3-HF, and those for Hf isotopic analysis were digested using alkali fusion method. Normalizing factors used to correct the mass bias of Nd—Hf during the measurements are $^{146}Nd/^{144}Nd = 0.7219$ and $^{179}Hf/^{177}Hf = 0.7325$, respectively.

Zircon U—Pb analyses were performed on the CAMECA ims-1280HR ion microprobe. A primary ion beam of O^{2-} was accelerated at −13 kv, with intensity of ca. 10 nA. The ellipsoidal spot size was ca. 20 μm × 30 μm. Detailed analytical procedures are similar to those described by Li et al. (2013). In order to monitor the external uncertainties of SIMS U—Pb measurements, analyses of an inner zircon standard Qinghu were interspersed with unknowns that were mounted in three mounts, yielding the weighted mean $^{206}Pb/^{238}U$ ages of 159.8 ± 1.8 Ma ($n = 7$), 159.5 ± 1.4 Ma ($n = 11$) and 158.2 ± 1.4 Ma ($n = 12$), respectively, which are identical within errors to the reported age of 159.5 ± 0.2 Ma (Li et al., 2013). Data reduction and age calculation were carried out using Isoplot program (version 4.15; Ludwig, 2003).

Zircon oxygen isotopic analyses were performed on CAMECA ims-1280HR and detailed analytical procedures were described in Yang et al. (2018). Data were corrected for instrumental mass fractionation (IMF) using a "standard-samples-standard" bracketing external standardization method. The Penglai zircon was used as the external standard and the reference zircon (Qinghu) was used as unknowns. Oxygen isotope ratios are reported in standard permil notation relative to Vienna Standard Mean Ocean Water (VSMOW). Qinghu zircon standard in this study yielded weighted mean $\delta^{18}O = 5.56 \pm 0.21‰$ (2σ; n = 7), 5.49 ± 0.47‰ (2σ; $n = 6$) and 5.24 ± 0.32‰ (2σ; $n = 8$) for three mounts, respectively, which are consistent with the reference values of 5.4 ± 0.2‰ (2σ) within errors (Li et al., 2013).

In situ zircon Lu—Hf isotopic analyses were conducted using a Neptune plus MC-ICP-MS equipped with a RESOlution M-50193 nm laser ablation system. The laser beam size was 45 μm and the repetition rate of 6 Hz at 4 J/cm^2 was used. Helium was chosen as the carrier gas (800 ml/min). Each analysis consisted of 300 cycles with an integration time of 50s. The detailed data reduction procedure is described in Zhang, Ren, Xia, Li, and Zhang (2015). Plešovice served as reference material. During Hf analysis, $^{176}Hf/^{177}Hf = 0.282483 \pm 30$ (2SD; $n = 20$), which is consistent with the reference value of $^{176}Hf/^{177}Hf = 0.282483 \pm 35$ (2SD; Sláma et al., 2008).

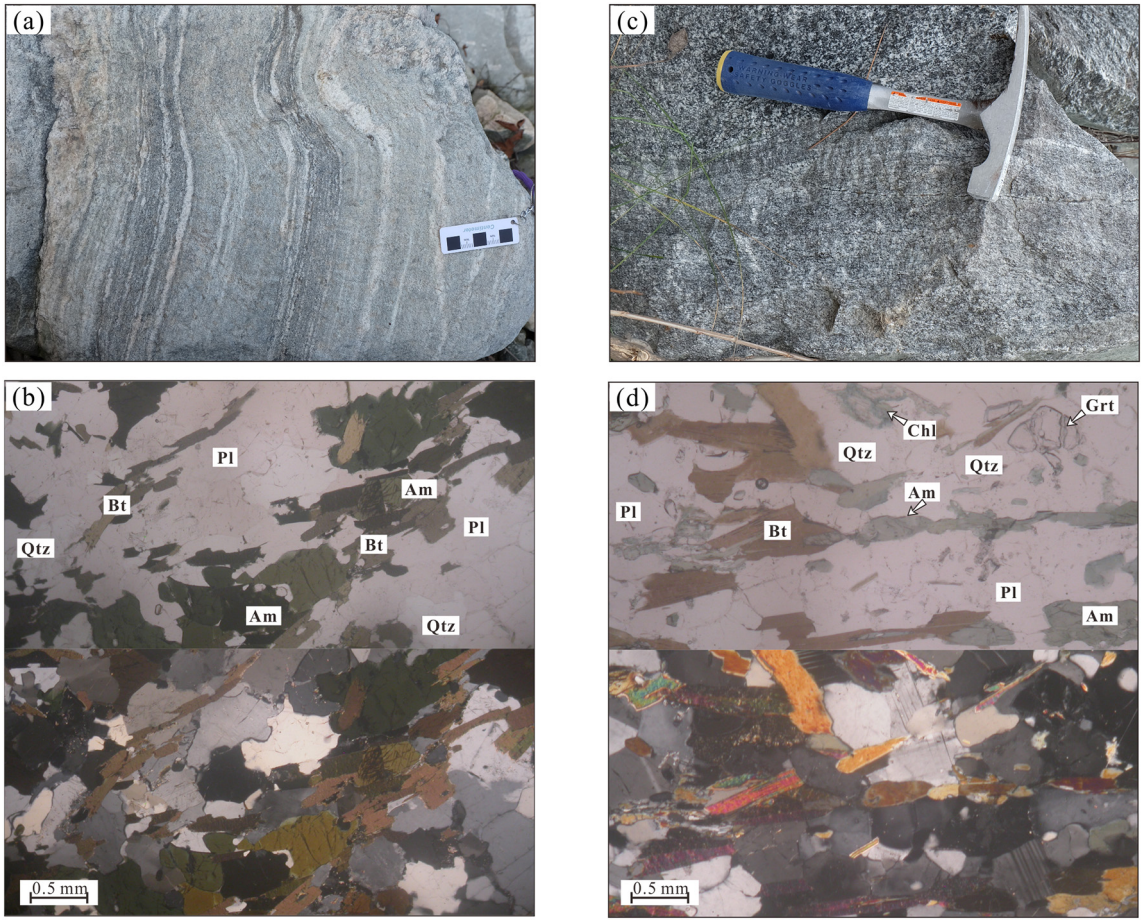

Fig. 2. Field photographs of the Taihua Complex in the Xiaoqinling area and petrographic characteristics of gneiss samples. (a) Banded gneiss sample exhibiting strong folding from the Jialu area; (b) photomicrograph of sample TH14150 from the Xitongyu area; the length of hammer is 28 cm; (c) gray gneiss with a weak gneissose structure from the Bayuan area; and (d) photomicrograph of sample TH14100 from the Bayuan area. Mineral abbreviations: Am = amphibole, Grt = garnet, Pl = plagioclase, Qtz = Quartz, Bt = Biotite, Chl = Chlorite.

4. Results

4.1. Zircon U—Pb ages

Gneiss samples from the Bayuan, Fushuizhen, Jialu, Xitongyu, Tizigou, and Laohugou locations (TH14100, TH14130, TH14141, TH14147, TH14155, and TH14160, respectively) were selected for in situ zircon U—Pb dating, and were collected from the Taihua Complex in the western to eastern Xiaoqinling area (Fig. 1c).

Zircons from sample TH14100 (Bayuan; 34°09′04“ N, 109°38’53” E) are euhedral-subhedral prismatic grains (Fig. 3a). The cathodoluminescence (CL) images revealed well-developed oscillatory zoning in the zircon cores, indicating a magmatic origin, but the rims are unzoned (Fig. 3a). Seventeen analyses of the oscillatory zoned cores have high U—Th contents (295–1703 and 121–599 ppm, respectively), with high Th/U ratios of 0.31–0.70 (Supplementary Table 1). These zircons yielded a weighted-mean $^{207}Pb/^{206}Pb$ age of 2296 ± 8 Ma, which is interpreted to be the crystallization age of the Bayuan gneiss (Fig. 3b).

Zircons from sample TH14130 (Fushuizhen; 34°30′00“ N, 109°57’51” E) are mostly euhedral prismatic grains and exhibit well-developed oscillatory zoning (Fig. 3c). Thirteen analyses of the zoned zircon domains have variable U—Th contents (204–1238 and 133–724 ppm, respectively), with Th/U ratios of 0.34–1.11 (Supplementary Table 1). Three analyses (Spots 8.1, 10.1, and 13.1) have old apparent $^{207}Pb/^{206}Pb$ ages (2506 ± 9, 2601 ± 28, and 2517 ± 4 Ma, respectively), and are inherited zircons. The other 10 analyses have variable apparent $^{207}Pb/^{206}Pb$ ages of 2378–2340 and 2452–2423 Ma, yielding weighted-mean $^{207}Pb/^{206}Pb$ ages of 2362 ± 17 and 2442 ± 20 Ma, respectively (Fig. 3d; Supplementary Table 1). The young age of 2362 ± 17 Ma is interpreted to be the crystallization age of the Fushuizhen gneiss, whereas the older age represents inherited zircons (Fig. 3d; Supplementary Table 1).

Zircons from sample TH14141 (Jialu; 34°24′14“ N, 110°07’10” E) are mostly stubby grains and exhibit oscillatory zoning (Fig. 3e). Fourteen analyses of the zoned zircon domains have moderate to high U—Th contents (120–2164 and 61.8–630 ppm, respectively), with Th/U ratios of 0.29–0.71 (Supplementary Table 1). These analyses yield apparent $^{207}Pb/^{206}Pb$ ages of 2286 ± 11 to 2340 ± 7 Ma and defined a weighted-mean $^{207}Pb/^{206}Pb$ age of 2323 ± 7 Ma, which is identical to the upper intercept age, and is interpreted as being the crystallization age of the Jialu gneiss (Fig. 3f).

Zircons from sample TH14147 (Xitongyu; 34°24′55“ N, 110°10’46” E) are mostly euhedral and prismatic grains. The CL images revealed oscillatory zoning in the zircon cores, whereas the rims are darker and unzoned (Fig. 3g). Fourteen analyses of the oscillatory zoned cores have moderate U—Th contents (105–749 and 28.7–615 ppm, respectively), with high Th/U ratios of 0.27–0.82, indicative of a magmatic origin. These zircons have a narrow range of apparent $^{207}Pb/^{206}Pb$ ages from 2332 ± 6 to 2316 ± 11 Ma, and yielded a weighted-mean age of 2325 ± 4 Ma (Fig. 3h; Supplementary Table 1), which is interpreted to be the crystallization age of the Xitongyu gneiss. Spot 5.2 on a zircon rim yielded a younger apparent $^{207}Pb/^{206}Pb$ age of 2284 ± 5 Ma, which probably reflects a later tectono-thermal event or a mixed age (Fig. 3g–h). In addition, three further analyses on zircon rims have high U and low Th contents (667–793 and 3.18–3.67 ppm, respectively) and very low Th/U ratios (0.004–0.005; Supplementary Table 1). These zircons

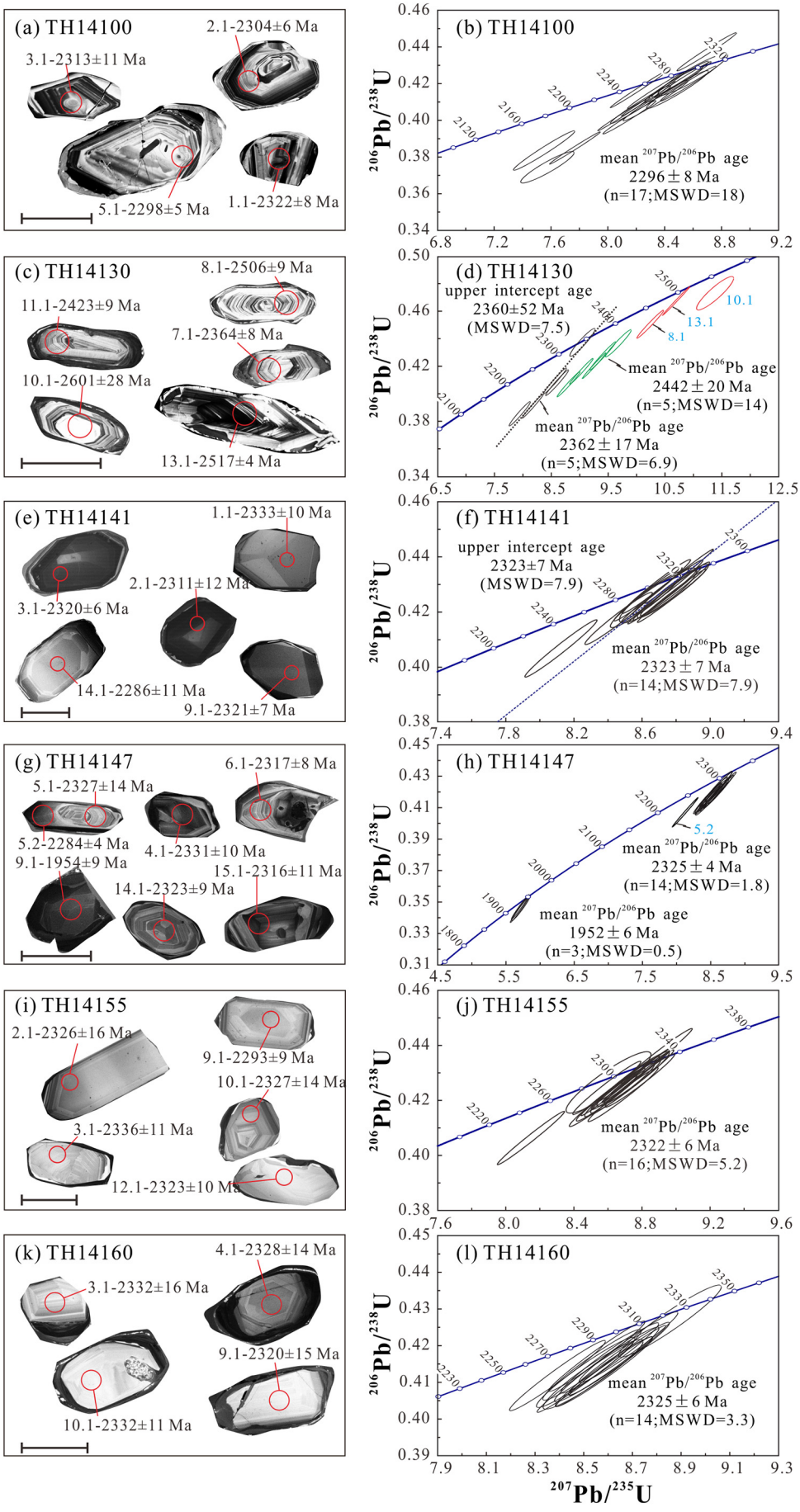
(a) TH14100
2.1-2304±6 Ma
3.1-2313±11 Ma
5.1-2298±5 Ma
1.1-2322±8 Ma
(b) TH14100
mean 207Pb/206Pb age
2296±8 Ma
(n=17;MSWD=18)
(c) TH14130
8.1-2506±9 Ma
11.1-2423±9 Ma
7.1-2364±8 Ma
10.1-2601±28 Ma
13.1-2517±4 Ma
(d) TH14130
upper intercept age
2360±52 Ma
(MSWD=7.5)
mean 207Pb/206Pb age
2442±20 Ma
(n=5;MSWD=14)
mean 207Pb/206Pb age
2362±17 Ma
(n=5;MSWD=6.9)
(e) TH14141
1.1-2333±10 Ma
2.1-2311±12 Ma
3.1-2320±6 Ma
14.1-2286±11 Ma
9.1-2321±7 Ma
(f) TH14141
upper intercept age
2323±7 Ma
(MSWD=7.9)
mean 207Pb/206Pb age
2323±7 Ma
(n=14;MSWD=7.9)
(g) TH14147
6.1-2317±8 Ma
5.1-2327±14 Ma
5.2-2284±4 Ma
4.1-2331±10 Ma
9.1-1954±9 Ma
15.1-2316±11 Ma
14.1-2323±9 Ma
(h) TH14147
mean 207Pb/206Pb age
2325±4 Ma
(n=14;MSWD=1.8)
mean 207Pb/206Pb age
1952±6 Ma
(n=3;MSWD=0.5)
(i) TH14155
2.1-2326±16 Ma
9.1-2293±9 Ma
10.1-2327±14 Ma
3.1-2336±11 Ma
12.1-2323±10 Ma
(j) TH14155
mean 207Pb/206Pb age
2322±6 Ma
(n=16;MSWD=5.2)
(k) TH14160
4.1-2328±14 Ma
3.1-2332±16 Ma
9.1-2320±15 Ma
10.1-2332±11 Ma
(l) TH14160
mean 207Pb/206Pb age
2325±6 Ma
(n=14;MSWD=3.3)
206Pb/238U
207Pb/235U

have younger apparent $^{207}Pb/^{206}Pb$ ages with a weighted-mean age of 1952 ± 6 Ma, which is considered to reflect the timing of metamorphism.

Zircons from sample TH14155 (Tizigou; 34°24′06" N, 110°17′00" E) are euhedral-subhedral and prismatic or stubby grains. The CL images revealed oscillatory zoning in the zircon cores, and the rims are dark and thin (Fig. 3i). Nineteen analyses on the oscillatory zoned cores have variable U—Th contents (106–688 and 47.8–355 ppm, respectively), with Th/U ratios of 0.44–0.73 (Supplementary Table 1). The apparent $^{207}Pb/^{206}Pb$ ages of the zircon cores vary between 2293 ± 9 and 2339 ± 13 Ma, corresponding to a weighted-mean age of 2322 ± 6 Ma, which is interpreted to be the crystallization age of the Tizigou gneiss (Fig. 3j; Supplementary Table 1).

Zircons from sample TH14160 (Laohugou; 34°22′44" N, 110°28′37" E) are euhedral and stubby. The CL images showed that most of the zircons have well-developed oscillatory zoning in their cores and dark rims (Fig. 3k). Fourteen analyses on oscillatory zoned cores have moderate U—Th contents (92.4–384 and 54.1–247 ppm, respectively), with high Th/U ratios of 0.34–0.82 (Supplementary Table 1). These zircons have apparent $^{207}Pb/^{206}Pb$ ages of 2300 ± 11 to 2334 ± 12 Ma, with a weighted-mean $^{207}Pb/^{206}Pb$ age of 2325 ± 6 Ma, which is interpreted to be the crystallization age of the Laohugou gneiss (Fig. 3l).

4.2. In situ zircon Hf—O isotopes

Zircon Hf—O isotope analyses were carried out at sites in the zircons that had been dated (Supplementary Table 2). Initial Hf isotope ratios were calculated based on the apparent $^{207}Pb/^{206}Pb$ ages ($t_{7/6}$) for each analytical site.

Igneous zircons from sample TH14100 have $\delta^{18}O$ values of 5.03‰–6.76‰, with a mean value of 6.14 ± 0.38‰ (Fig. 4a; Supplementary Table 2). The $^{176}Hf/^{177}Hf$ ratios vary from 0.281148–0.281370, with corresponding slightly positive to negative $\varepsilon_{Hf}(t_{7/6})$ values (−6.38 to +1.13), and variable two-stage Hf model ages of 2.78–3.25 Ga (Fig. 4b; Supplementary Table 2).

Igneous zircons from sample TH14141 have relatively lower $\delta^{18}O$ values (3.97‰–5.09‰; mean = 4.51 ± 0.29‰; Supplementary Table 2) as compared with sample THB14100 (Fig. 4a; Supplementary Table 2). These zircons have a relatively narrow range of $^{176}Hf/^{177}Hf$ ratios (0.281198–0.281243), with negative $\varepsilon_{Hf}(t_{7/6})$ values (−4.94 to −2.84), and two-stage Hf model ages of 3.04–3.18 Ga (Fig. 4b; Supplementary Table 2).

For sample TH14147, 15 analyses of oscillatory zoned zircon cores have $\delta^{18}O$ values of 4.72‰–6.35‰, with a mean value of 5.21 ± 0.21‰ (Fig. 4a; Supplementary Table 2). These zircons have relatively low $^{176}Hf/^{177}Hf$ ratios (0.281248–0.281377), slightly positive to negative initial $\varepsilon_{Hf}(t_{7/6})$ values (−5.23 to +0.27), and old two-stage Hf model ages of 2.85–3.19 Ga (Fig. 4b; Supplementary Table 2). Three late Paleoproterozoic metamorphic zircons (1.95 Ga) have slightly lower $\delta^{18}O$ values of 4.11‰–4.41‰ (Supplementary Table 2).

Igneous zircons from sample TH14155 have $^{176}Hf/^{177}Hf$ ratios between 0.281280 and 0.281370, corresponding to $\varepsilon_{Hf}(t_{7/6})$ values from −2.52 to +1.62 and two-stage Hf model ages of 2.77–3.02 Ga (Fig. 4b; Supplementary Table 2).

Igneous zircons from sample TH14160 have $\delta^{18}O$ values of 6.19‰–6.79‰, with a mean value of 6.53 ± 0.10‰ (Fig. 4a; Supplementary Table 2). These zircons have $^{176}Hf/^{177}Hf$ ratios of 0.281271–0.281377, with $\varepsilon_{Hf}(t_{7/6})$ values of −1.50 to +1.94 and two-stage Hf model ages of 2.75–2.95 Ga (Fig. 4b; Supplementary Table 2).

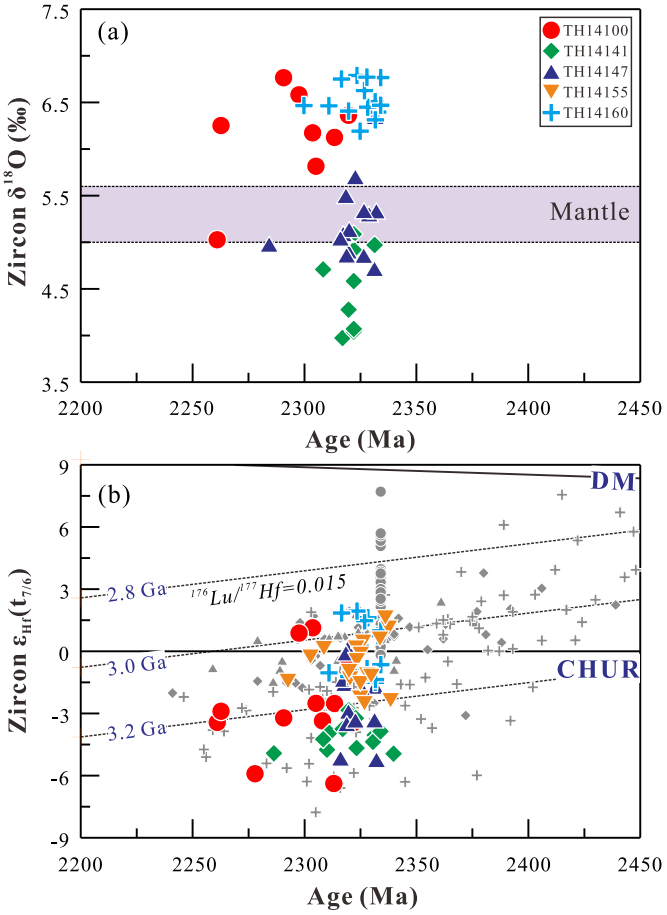

Fig. 4. Plots of zircon (a) $\delta^{18}O$ and (b) $\varepsilon_{Hf}(t)$ versus age for gneisses from the Taihua Complex. Literature data (gray) are from Diwu, Sun, Zhao, and Lai (2014), Huang, Wilde, and Zhong (2013), Jia et al. (2019), and Yu, Liu, Li, Chen, and Dai (2013). $\delta^{18}O$ range for mantle zircons (5.3‰ ± 0.3‰) from Valley, Kinny, Schulze, and Spicuzza (1998).

4.3. Whole-rock major and trace elements

The studied samples have variable SiO_2 (56.70–71.40 wt%), MgO (0.45–3.61 wt%), and K_2O (1.00–5.86 wt%; Fig. 5a–b) contents, and variable trace element concentrations (Figs. 5–6; Supplementary Table 3). Based on major and trace elements, the studied samples can be broadly subdivided into three suites (Group-1, −2, and − 3; Figs. 5–6).

Group-1 samples are high-K_2O gneisses from the Dumutai, Fushuizhen, and Tizigou areas, which belong mostly to the shoshonite series (Fig. 5b) and plot in the fields for granite and monzonite in the Ab–Or–An diagram (Fig. 5c). These gneisess have fractionated REE patterns ($[La/Yb]_N$ = 35.1–168) and negative Eu—Sr anomalies (Fig. 6; Supplementary Table 3). Group-2 samples are relatively low-K_2O gneisses from the Jialu, Xitongyu, Dumutai, Tizigou, and Laohugou areas (Fig. 5b), which plot mostly in the fields for tonalite and granodiorite in the Ab–Or–An diagram (Fig. 5c). These gneisses have less fractionated REE patterns ($[La/Yb]_N$ = 6.85–43.2) than the Group-1 gneisses, no Eu anomalies, and significant negative Nb, Ta, and Ti anomalies in a primitive-mantle-normalized multi-element diagram (Fig. 6; Supplementary Table 3). Group-3 samples are high-MgO, —Cr, and —Ni gneisses from the Bayuan area (Fig. 5a, d, and e), which plot mostly in the field for tonalite in the Ab–Or–An diagram (Fig. 5c). These

Fig. 3. Representative cathodoluminescence images of zircons and concordia diagrams for gneisses from the Taihua Complex: (a–b) TH14100; (c–d) TH14130; (e–f) TH14141; (g–h) TH14147; (i–j) TH14155; (k–l) TH14160. Scale bar is 100 μm and analyzed spot diameter is 30 μm.

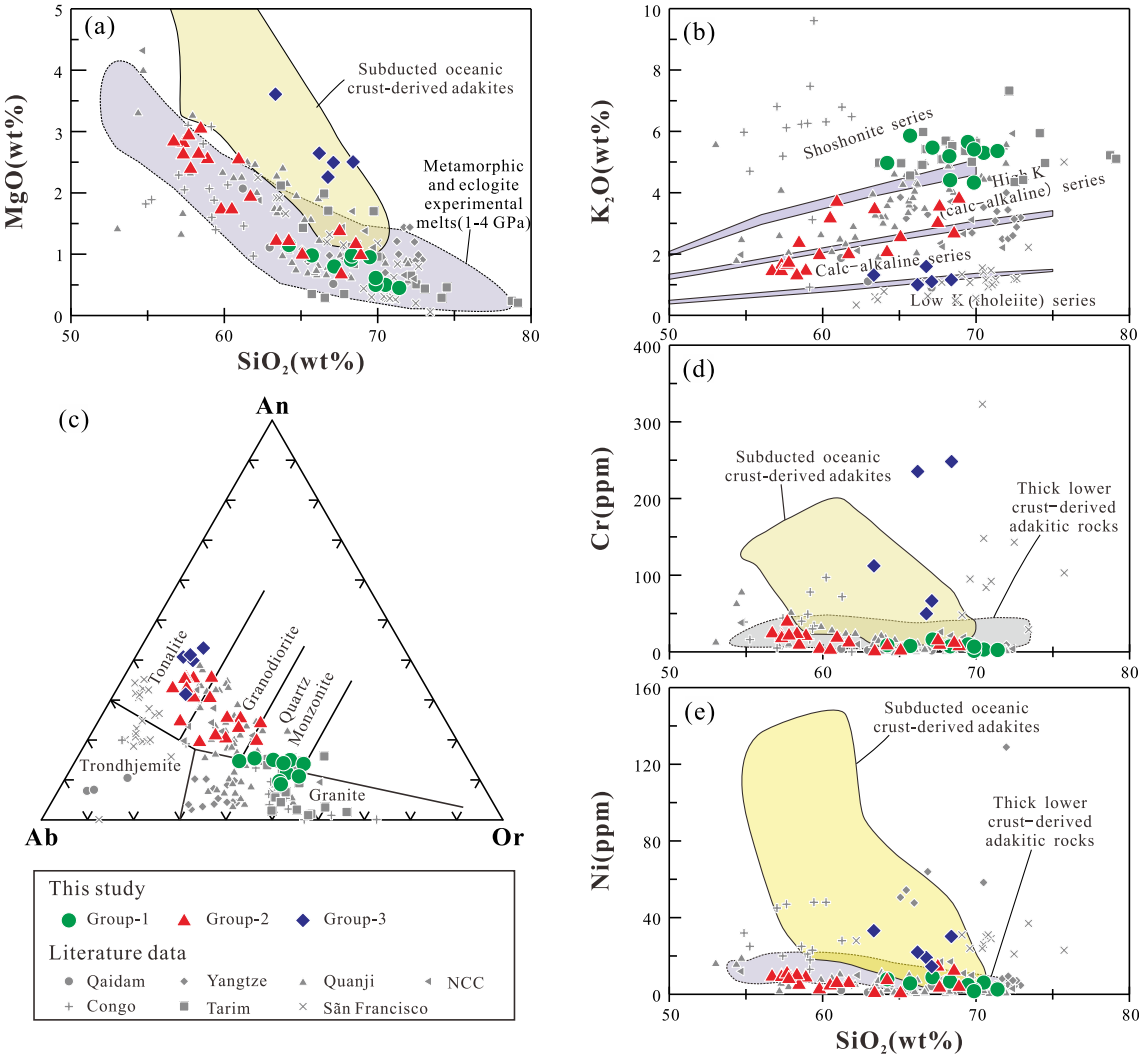

Fig. 5. (a–b) Plots of MgO and K_2O versus SiO_2; (c) An–Ab–Or classification diagram (Barker and Arth, 1976); and (d–e) plots of Cr and Ni versus SiO_2 for gneisses from the Taihua Complex. Fields of subducted oceanic crust-derived adakites and metabasaltic and eclogite experimental melts are after the compilations of Wang et al. (2006). Literature data from the Qaidam Basin (Yu, Fu, Wang, Li, and Guo, 2017), Yangtze Block (Cui et al., 2019), Quanji Massif (Gong et al., 2014; Gong, He, Wang, Chen, and Kusky, 2019; He et al., 2018), and the São Francisco (Seixas, David, and Stevenson, 2012; Teixeira et al., 2015), Congo (Tchameni, Mezger, Nsifa, and Pouclet, 2001), Tarim (Zhang, Li, Li, Yu, and Ye, 2007), and North China (Huang, Wilde, Yang, and Zhong, 2012) cratons.

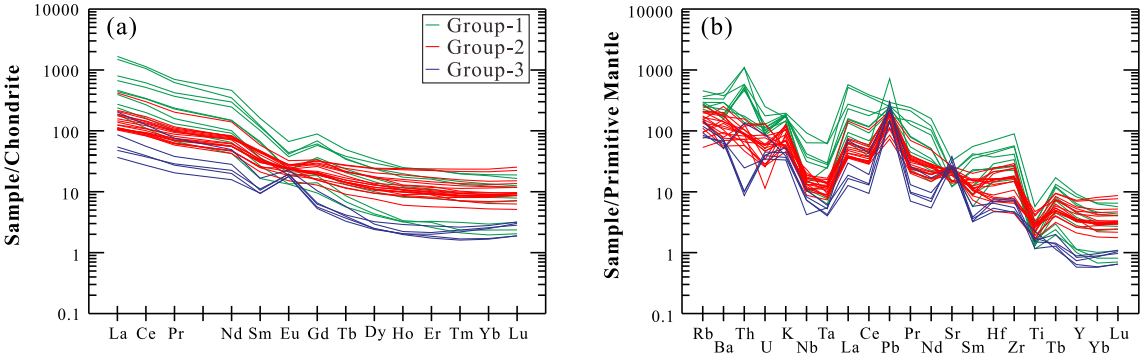

Fig. 6. Chondrite-normalized REE patterns and primitive-mantle-normalized multi-element diagrams for gneisses from the Taihua Complex. Chondrite and primitive mantle normalizing values from Sun and McDonough (1989).

gneisses have highly fractionated REE patterns ($[La/Yb]_N = 17.2–79.5$), marked positive Eu−Sr anomalies, and overall lower trace element concentrations compared with the other samples (Fig. 6; Supplementary Table 3).

4.4. Whole-rock Hf—Nd isotopes

Group-1 samples have variable $^{143}Nd/^{144}Nd$ (0.510779–0.510783) and $^{176}Hf/^{177}Hf$ (0.281326–0.281550) ratios, with variable initial

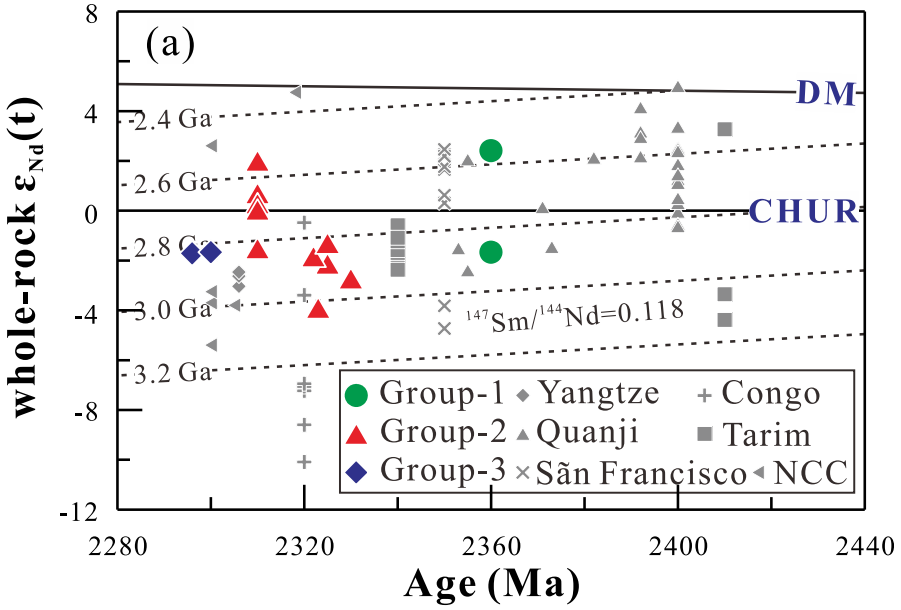
(a)
DM
CHUR
2.4 Ga
2.6 Ga
2.8 Ga
3.0 Ga
3.2 Ga
147Sm/144Nd=0.118
Group-1
Group-2
Group-3
Yangtze
Quanji
Sãn Francisco
Congo
Tarim
NCC
whole-rock εNd(t)
Age (Ma)

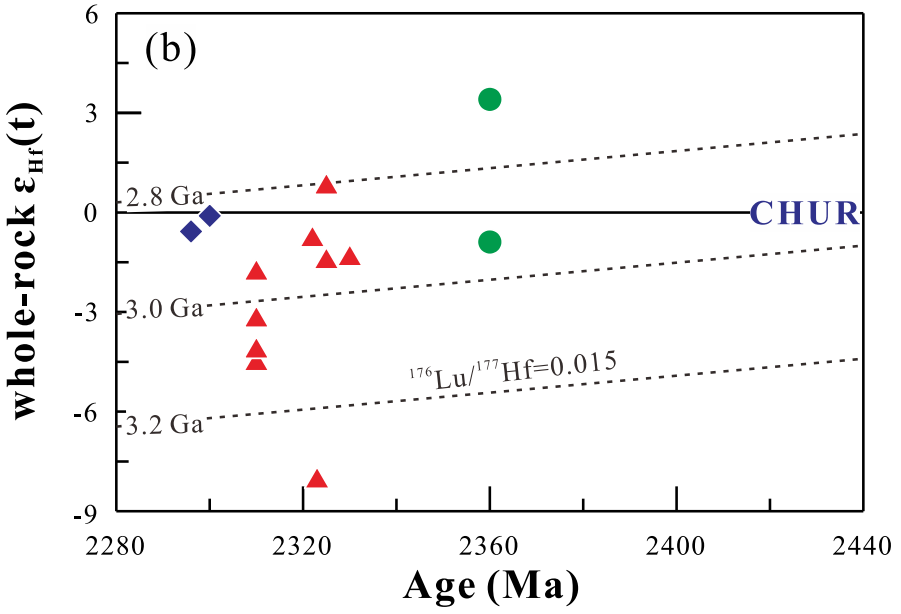
(b)
CHUR
2.8 Ga
3.0 Ga
3.2 Ga
176Lu/177Hf=0.015
whole-rock εHf(t)
Age (Ma)

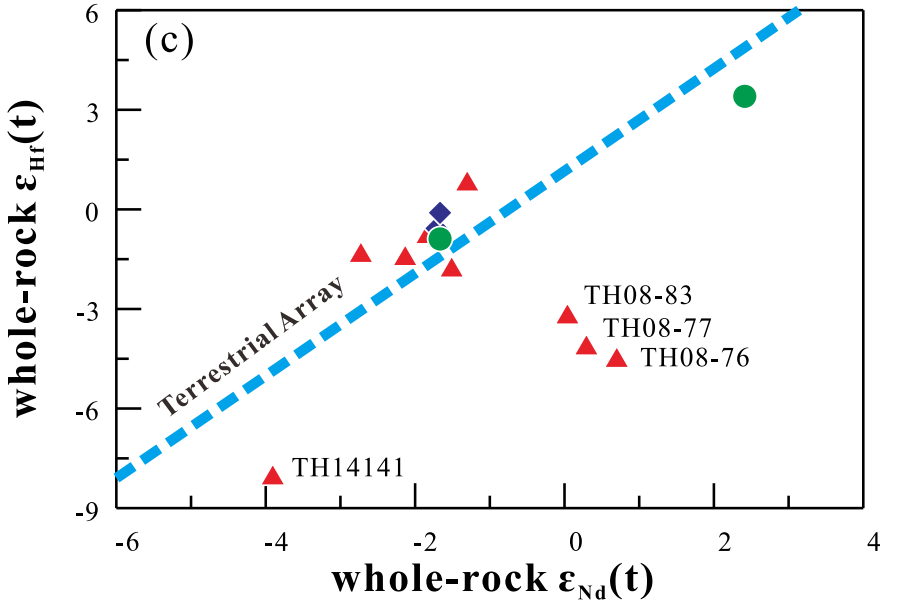
(c)
Terrestrial Array
TH08-83
TH08-77
TH08-76
TH14141
whole-rock εHf(t)
whole-rock εNd(t)

$\varepsilon_{Nd}(t)$ (−1.67 to +2.41) and $\varepsilon_{Hf}(t)$ values (−0.89 to +3.41) and Nd −Hf model ages ($T_{DM\text{-}Nd}$ = 2.49–2.74 Ga; $T_{DM2\text{-}Nd}$ = 2.56–2.90 Ga; $T_{DM\text{-}Hf}$ = 2.58–2.73 Ga; $T_{DM2\text{-}Hf}$ = 2.68–2.95 Ga; Fig. 7; Supplementary Table 4).

Group-2 samples have variable $^{143}Nd/^{144}Nd$ ratios (0.511047–0.511420) and initial $\varepsilon_{Nd}(t)$ values (−3.91 to +2.00), corresponding to variable Nd model ages ($T_{DM\text{-}Nd}$ = 2.52–3.02 Ga; $T_{DM2\text{-}Nd}$ = 2.56–3.05 Ga) that are older than their crystallization ages (Fig. 7a; Supplementary Table 4). These samples also have low $^{176}Hf/^{177}Hf$ ratios of 0.281411–0.281855, corresponding to slightly positive to negative initial $\varepsilon_{Hf}(t)$ values (−7.99 to +0.87) and variable Hf model ages ($T_{DM\text{-}Hf}$ = 2.65–3.41 Ga; $T_{DM2\text{-}Hf}$ = 2.81–3.35 Ga; Fig. 7b; Supplementary Table 4). In addition, data for samples TH14141, TH08–76, TH08–77, and TH08–83 diverge from the terrestrial array defined by Vervoort, Plank, and Prytulak (2011), with lower $^{176}Hf/^{177}Hf$ relative to $^{143}Nd/^{144}Nd$ (Fig. 7c).

Group-3 samples have low $^{143}Nd/^{144}Nd$ ratios (0.511071–0.511395), corresponding to negative initial $\varepsilon_{Nd}(t)$ values (−1.71 and − 1.67) and old Nd model ages ($T_{DM\text{-}Nd}$ = 2.75–2.85 Ga; $T_{DM2\text{-}Nd}$ = 2.85 Ga; Fig. 7a; Supplementary Table 4). These samples have low $^{176}Hf/^{177}Hf$ ratios of 0.281452–0.281518, corresponding to negative initial $\varepsilon_{Hf}(t)$ values (−0.10 to −0.57) and old Hf model ages ($T_{DM\text{-}Hf}$ = 2.67–2.70 Ga; $T_{DM2\text{-}Hf}$ = 2.85–2.88 Ga; Fig. 7b; Supplementary Table 4).

5. Discussion

5.1. Petrogenesis of granitoid gneisses in the Taihua Complex

Group-1 gneisses are characterized by fractionated REE patterns (e.g., high La/Yb and Dy/Yb ratios), which might reflect partial melting of a deep source with residual garnet. Residual garnet would significantly increase the La/Yb and Dy/Yb ratios of the melt, because it has progressively increasing partition coefficients for REEs with increasing atomic number (Moyen, 2009; Moyen and Martin, 2012). However, the Group-1 gneisses have relatively low Sr contents, low Sr/Y ratios, and negative Eu anomalies (Figs. 6 and 8), indicating plagioclase was a residual phase during partial melting, which requires relatively low-pressure conditions. In addition, the high-K_2O gneisses from the Dumutai area have relatively high zircon saturation temperatures (805–973 °C; Jia, 2016), which likely reflect partial melting of the middle–lower crust under high-temperature–low-pressure conditions (Jia, 2016). Thus, the high La/Yb and Dy/Yb ratios of the Group-1 gneisses were inherited from a source characterized by high La/Yb and Dy/Yb ratios, such as preexisting TTGs; however, partial melting experiments have shown that TTGs are typically too sodic to produce potassic magmas (Watkins, Clemens, and Treloar, 2007). Therefore, the source of the Group-1 gneisses requires the involvement of K-rich materials. Given that the Group-1 samples are silicic rocks with relatively low MgO and Fe_2O_3 contents (Fig. 5; Supplementary Table 3), these cannot be an analogue of high-Mg andesites derived from a highly enriched and metasomatized mantle source (Rapp, Shimizu, Norman, and Applegate, 1999). Therefore, the protoliths of the Group-1 gneisses were partial melts of pre-existing TTGs that were hybridized with a high-K component (i.e., evolved crustal materials or K-rich magmas; Laurent, Martin, Moyen, and Doucelance, 2014; Nelson, 1992) at high-temperature–low-pressure conditions.

Group-2 gneisses have relatively high Y and heavy REE contents, with low La/Yb, Dy/Yb, and Sr/Y ratios (Figs. 6 and 8), and are different from TTGs. Such geochemical features preclude the involvement of garnet in the petrogenesis of these gneisses. In addition, these samples have relatively uniform La/Yb and Dy/Yb ratios (Fig. 8) and variable SiO_2 contents (Fig. 5; Supplementary Table 3), which cannot be explained by magmatic differentiation, but likely reflect partial melting processes. The Group-2 samples have slightly positive to negative zircon $\varepsilon_{Hf}(t_{7/6})$ and whole-rock $\varepsilon_{Nd}(t)$ and $\varepsilon_{Hf}(t)$ values, implying an ancient crustal source. Thus, the protoliths of the Group-2 gneisses could have been derived by partial melting of an ancient crustal source without garnet in the residue.

Group-3 gneisses have relatively low REE and Y abundances, marked positive Eu anomalies (Fig. 6a), and moderate to high La/Yb and Sr/Y ratios (Fig. 8), and plot in the fields for adakite and high-Al TTGs on diagrams of $[La/Yb]_N$ versus Yb_N and Sr/Y versus Y (Fig. 8a–b; Supplementary Table 3). High Sr/Y ratios (Fig. 8b and d) and positive Eu anomalies (Fig. 6a) are due to plagioclase accumulation (Qian and Hermann, 2013), which is consistent with the positive correlation between Sr/Y and Eu/Eu^* (Fig. 8d). In addition, Group-3 samples exhibit depletions in heavy REEs and high La/Yb ratios, indicating that residual garnet ± amphibole was present in the source during partial melting. Given that amphibole has higher partition coefficients for middle REEs than heavy REEs (Moyen, 2009; Moyen and Martin, 2012), its presence in the source will produce high La/Yb and low Dy/Yb ratios in the melt. The studied samples have low Dy/Yb ratios, but there is no correlation between La/Yb and Dy/Yb ratios (Fig. 8c), which could be attributed to the presence of residual garnet and amphibole during partial melting. Residual garnet and amphibole require partial melting at high pressures (Xiong, 2006; Xiong, Adam, and Green, 2005), which could be due to oceanic crustal subduction or lower crustal thickening and delamination (e.g., Condie, 2005; Smithies and Champion, 2000). Group-3 samples have high MgO, Cr, and Ni contents and plot mostly in the field for subducted oceanic crust-derived adakites (Fig. 5a, d, and e), which implies the significant involvement of mantle materials. However, these samples have slightly positive to negative zircon $\varepsilon_{Hf}(t_{7/6})$, and negative whole-rock $\varepsilon_{Nd}(t)$ and $\varepsilon_{Hf}(t)$ values (Figs. 4 and 7), indicating the magma source was mainly ancient crust rather than juvenile oceanic crust. Therefore, our preferred mechanism for generating the protoliths of the Group-3 gneisses involves the partial melting of delaminated lower crust.

5.2. Magmatic sources of the gneisses in the Taihua Complex based on zircon Hf—O isotopes

Given that it is a physically and chemically stable accessory mineral, zircon is a critical tool for understanding the evolution of continental crust (Cawood, Hawkesworth, and Dhuime, 2013; Hawkesworth and Kemp, 2006). Zircon Hf—O isotope data can reflect the relative contributions of the mantle and crust, thereby providing insights into crustal growth and reworking. Only a few studies have reported zircon O isotope data for early Precambrian rocks in the southern NCC (Diwu, Sun, Gao, and Fan, 2013; Liu et al., 2009). The available data show that the Archean zircons dominantly have mantle-like $\delta^{18}O$ values, whereas the early Paleoproterozoic zircons have higher $\delta^{18}O$ values, indicating the recycling of surface-derived materials (Diwu, Sun, Gao, and Fan, 2013; Liu et al., 2009).

Zircon can preserve its primary Hf—O isotopic composition despite high-grade metamorphism (Valley et al., 2005; Wu, Li, Zheng, and Gao, 2007), but O isotopes can be reset by dissolution–re-precipitation during metamictization (Booth et al., 2005). Magmatic zircons in the Taihua Complex should retain their primary O isotope signatures, because $\delta^{18}O$ values are not correlated with the degree of age discordance (Fig. 9a).

Fig. 7. Nd–Hf isotope evolution diagrams for gneisses from the Taihua Complex. (a) $\varepsilon_{Nd}(t)$ versus age; (b) $\varepsilon_{Hf}(t)$ versus age; (c) $\varepsilon_{Hf}(t)$ versus $\varepsilon_{Nd}(t)$. Terrestrial array from Vervoort, Plank, and Prytulak (2011).

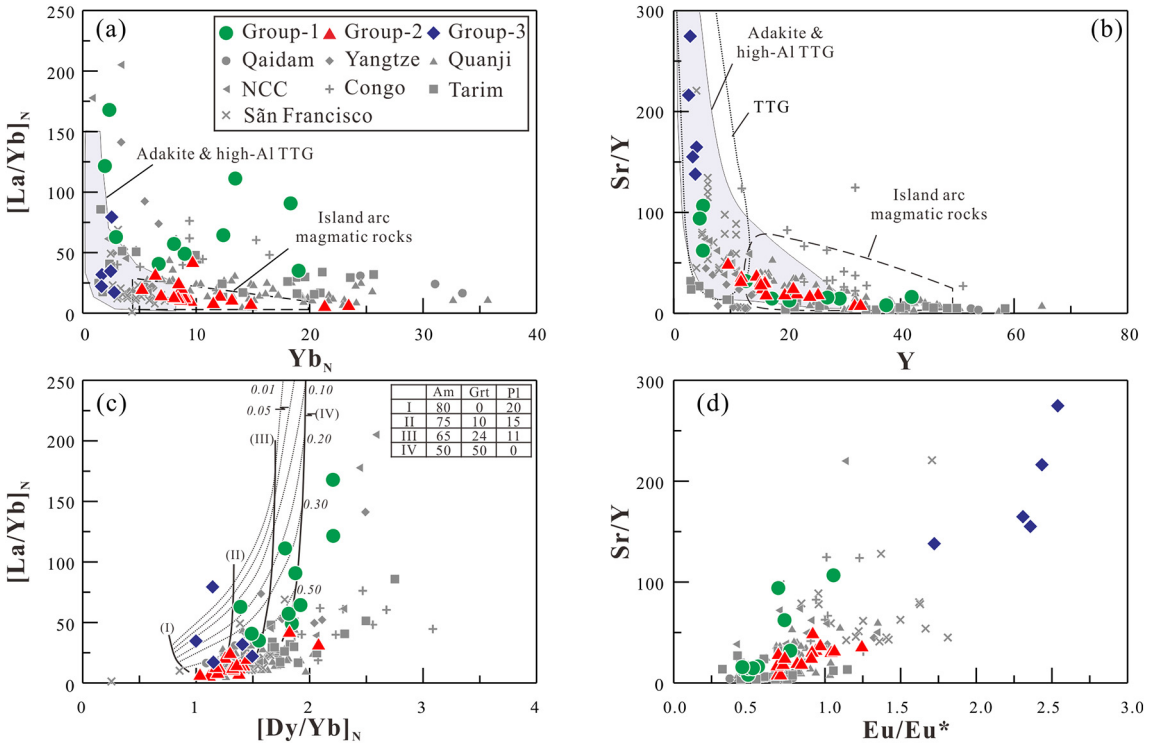

Fig. 8. Plots of (a) $[La/Yb]_N$ versus Yb_N; (b) Sr/Y versus Y; (c) $[La/Yb]_N$ versus $[Dy/Yb]_N$; and (d) Sr/Y versus Eu/Eu* for gneisses from the Taihua Complex. Fields for high-Al TTG, adakite, and island arc igneous rocks from Drummond and Defant (1990) and Martin, Smithies, Rapp, Moyen, and Champion (2005). Curves show the partial melting trends of sample TH14151. Partition coefficients from Johnson, Brown, Gardiner, Kirkland, and Smithies (2017). Mineral abbreviations: Am = amphibole, Grt = garnet, and Pl = plagioclase.

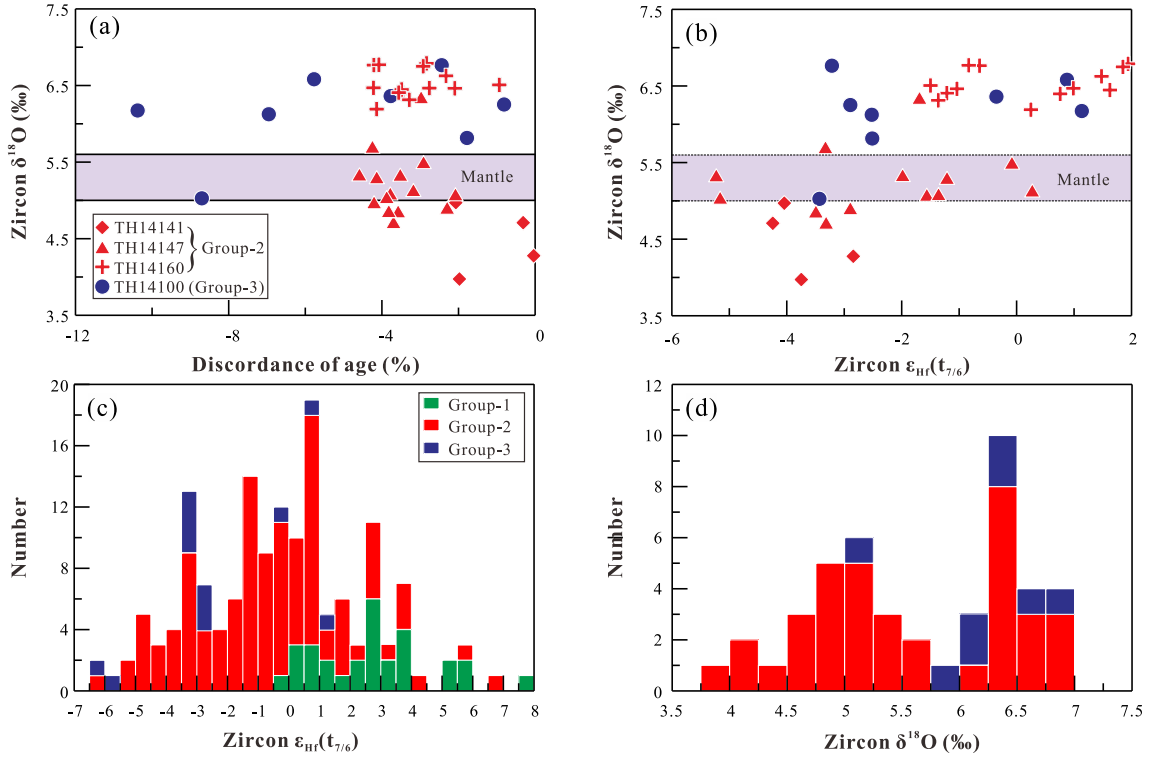

Fig. 9. *(a–b) Plots of zircon* $\delta^{18}O$ values versus age discordance and $\varepsilon_{Hf}(t_{7/6})$ *values; and (c–d) histograms of zircon* $\varepsilon_{Hf}(t_{7/6})$ *and* $\delta^{18}O$ *values for gneisses from the Taihua Complex.* Data from Huang, Wilde, and Zhong (2013), Jia (2016), Jia et al. (2019), and this study.

Igneous zircons from Group-1 samples are characterized by near- to super-chondritic Hf isotopic compositions with $\varepsilon_{Hf}(t_{7/6})$ values of −0.18 to +7.70 (Fig. 9c), suggesting a dominant juvenile crustal source. However, the Group-1 samples have variable whole-rock $\varepsilon_{Nd}(t)$ and $\varepsilon_{Hf}(t)$ values (Fig. 7), indicating the involvement of ancient crustal materials. Sample TH14130 contains inherited zircons with apparent $^{207}Pb/^{206}Pb$ ages of 2601 ± 28 to 2423 ± 9 Ma, also requiring the involvement of pre-existing crustal materials. Therefore, the protoliths of the Group-1 gneisses may have been a mixed source of juvenile and ancient crust materials.

Igneous zircons from Group-2 gneisses have variable $\varepsilon_{Hf}(t_{7/6})$ values from −6.15 to +6.55, but most are sub-chondritic in composition (Fig. 9c). This and the slightly positive to negative whole-rock $\varepsilon_{Nd}(t)$ and $\varepsilon_{Hf}(t)$ values (Fig. 7) indicate that the protoliths of the Group-2 gneisses were formed by reworking of ancient crust with minor inputs from juvenile material. The zircons have variable $\delta^{18}O$ values (3.97‰–6.79‰; Supplementary Table 2) relative to the mantle value (5.3‰ ± 0.3‰; Valley, Kinny, Schulze, and Spicuzza, 1998), which also indicates the source was heterogeneous. Furthermore, zircons from sample TH14160 have higher $\delta^{18}O$ values (6.19‰–6.79‰) than the mantle value (Fig. 4a), which requires a source that has experienced low-temperature hydrothermal alteration (Valley et al., 2005; Wei, Zheng, Zhao, and Valley, 2002). In fact, high-$\delta^{18}O$ zircons became more prevalent since the end-Archean, probably in response to the onset of subduction and rate of recycling of surface-derived materials into the mantle (Ma et al., 2020; Valley et al., 2005). However, zircons from sample TH14141 have slightly lower $\delta^{18}O$ values (3.97‰–5.09‰) than the mantle value (Fig. 4a). These zircons have sub-chondritic Hf isotopes and negative $\varepsilon_{Hf}(t_{7/6})$ values (Fig. 4b), which do not correlate with O isotopes (Fig. 10b). This cannot be the result of assimilation of low-$\delta^{18}O$ rocks, and requires a pre-existing low-$\delta^{18}O$ source. High-temperature hydrothermally altered oceanic crust has relatively low $\delta^{18}O$ values (2‰–5‰) due to high-temperature fluid–rock interaction (Bindeman et al., 2005; Wei, Zheng, Zhao, and Valley, 2002). Thus, ancient altered oceanic crust might have been the source of the protoliths for the Group-2 gneisses, particularly given their enriched whole-rock Nd and Hf isotopic compositions. Furthermore, given that the upper part of altered oceanic crust typically has high $\delta^{18}O$ due to low-temperature hydrothermal alteration, this might have been the source for the high-$\delta^{18}O$ rocks.

Igneous zircons from Group-3 gneisses have variable $\varepsilon_{Hf}(t_{7/6})$ values (−6.38 to +1.13) that are mostly negative (Fig. 9c) and, together with the negative whole-rock $\varepsilon_{Nd}(t)$ and $\varepsilon_{Hf}(t)$ values (Fig. 7), this suggests that the protoliths may be the product of crustal reworking. In addition, the Group-3 gneisses have high MgO, Cr, and Ni contents, indicating the involvement of juvenile materials, which is also consistent with the slightly positive zircon $\varepsilon_{Hf}(t_{7/6})$ values of some samples (Fig. 9c). The elevated zircon $\delta^{18}O$ values (5.03‰–6.76‰) of the Group-3 gneisses suggest that their source might have experienced low-temperature hydrothermal alteration prior to partial melting.

In summary, igneous zircons in gneisses from the Taihua Complex mainly record crustal reworking along with subordinate crustal growth. The magmatic sources of the gneiss protoliths experienced hydrothermal alteration.

5.3. Implications for the early Paleoproterozoic tectonic setting of the southern NCC

There was a remarkable reduction in magmatic activity on Earth at 2.45–2.20 Ga, which was probably due to a global plate tectonic shutdown or slowdown (Condie, O'Neill, and Aster, 2009; Partin et al., 2014; Spencer, Murphy, Kirkland, Liu, and Mitchell, 2018). Prior to the tectono-magmatic shutdown, scattered continental blocks had been amalgamated into a supercontinent at 2.7–2.5 Ga (i.e., the Kenorland supercontinent; Aspler and Chiarenzelli, 1998), which might have been responsible for the global cessation or slowdown of plate tectonics (Condie, O'Neill, and Aster, 2009). During the tectono-magmatic shutdown, mafic-ultramafic magmatism occurred in response to a mantle

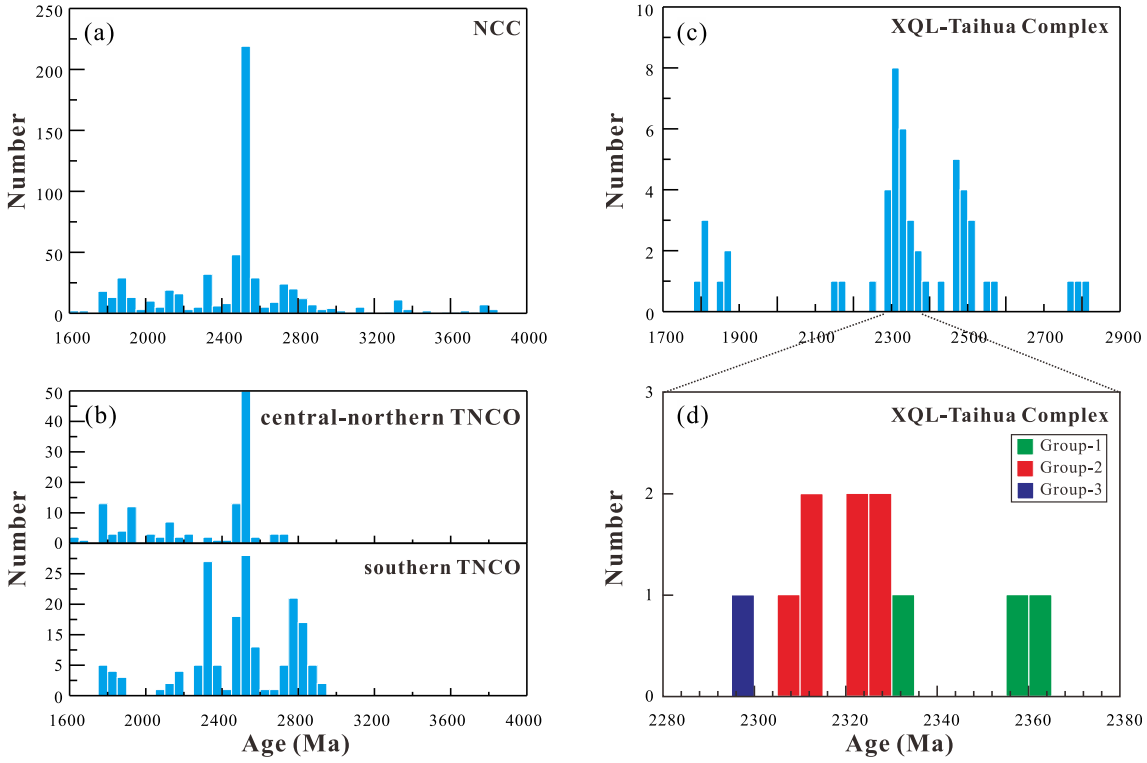

Fig. 10. *Histograms* of magmatic crystallization ages in the NCC, central–northern TNCO, southern TNCO, and Taihua Complex in the Xiaoqinling area. Data sources listed in Supplementary Table 5.

plume triggering the break-up of Kenorland (Eriksson and Condie, 2014; Partin et al., 2014, and references therein), suggesting that a global extensional setting prevailed. In contrast, coeval silicic (e.g., TTGs) and other arc-related magmatism was uncommon.

The NCC contains widespread Archean to Paleoproterozoic basement (Fig. 10a). The ca. 2.3 Ga magmatism was concentrated in the TNCO, although small amounts of magmatism occurred in the Western Block (Supplementary Table 5). Furthermore, early Paleoproterozoic magmatism in the southern TNCO was more extensive than that in the middle–northern TNCO (Fig. 10b). The Taihua Complex in the Xiaoqinling area is the largest exposure of Precambrian basement in the southern TNCO, and records episodes of magmatism at 2.80–1.80 Ga (Fig. 10c; Supplementary Table 5), and significant intermediate to silicic magmatism at ca. 2.3 Ga. This contrasts with the relatively rare silicic magmatism during the global tectono-magmatic shutdown. According to the zircon U—Pb age data and geochemical features of gneisses in the Xiaoqinling Taihua Complex, we propose a model for the formation of the silicic magmatism (Fig. 10d).

The earliest magmatism is represented by the Group-1 gneisses that are characterized by high K_2O contents (Fig. 5b), and were derived by partial melting with residual plagioclase in the source. Alongside their high zircon saturation temperatures (Jia et al., 2019), this indicates formation in a high-temperature–low-pressure extensional setting. Extensional tectonics favored the generation of K-rich magmas (Müller and Groves, 1997).

The subsequent magmatism represented by the Group-2 gneisses has less fractionated REE patterns (Fig. 6a) and low La/Yb and Dy/Yb ratios (Fig. 8c), indicating relatively shallow depths of partial melting without residual garnet in the source. Based on zircon Hf—O isotope data, ancient altered oceanic crust might have been the source for these rocks. Thus, relatively high degrees of partial melting were required to produce the low La/Yb and Dy/Yb ratios (Fig. 8c), which can also explain the relatively low SiO_2 and high FeO–MgO contents (Fig. 5a; Supplementary Table 3). In an extensional tectonic setting, mantle upwelling could have provided the thermal anomaly required for the high-degree partial melting of the ancient oceanic crust.

The youngest magmatism is represented by the Group-3 gneisses that have high MgO, Cr, and Ni contents (Fig. 5a, d, and e), and negative whole-rock $\varepsilon_{Nd}(t)$ and $\varepsilon_{Hf}(t)$ values (Fig. 7a–b). The protoliths of the Group-3 gneisses were formed by partial melting of delaminated lower crust. In general, delaminated lower crust is denser than the underlying mantle, which leads to gravitational instability (e.g., Johnson, Brown, and Kaus, 2013; Lustrino, 2005). In fact, the lower crust in the Xiaoqinling area would have experienced multiple stages of partial melting in the late Archean, which resulted in extensive TTG magmatism (Fig. 10c; Huang, Wilde, and Zhong, 2013; Jia et al., 2016, 2019). Thus, the lower crust would have been dense and eclogitic, and susceptible to delamination in the early Paleoproterozoic. In addition, a thermal anomaly and relatively low strain state in an extensional setting would also have facilitated delamination.

In summary, the geochronology and geochemistry of the Taihua Complex in the Xiaoqinling area records a process of orogenic collapse (i.e., extension to delamination) along the southern TNCO during the early Paleoproterozoic. Indeed, the southern TNCO, as an existing orogenic belt at ca. 2.3 Ga, was the weakened lithospheric zone during the orogenic collapse. Such a weakened zone would be the location of early expression of the orogenic collapse (i.e., partial melting of pre-existing TTG and K-rich rocks in an extensional setting), and also facilitate the lower crust delamination and subsequent mantle upwelling and remelting of ancient basement. In addition, integrated geochronological and geochemical data for the Taihua and Dengfeng complexes show that the southern TNCO experienced subduction–collision–accretion processes at the end of the Archean (e.g., Diwu, Sun, Zhao, and Lai, 2014; Huang, Wilde, and Zhong, 2013; Jia et al., 2016, 2019; Wang, Huang, and Yang, 2019; Wang, Huang, Yang, and Luo, 2017b). There is an emerging record of magmatism with ages ranging between ~2.45 and 2.22Ga on every continent, which argues for a dynamic plate tectonic regime with co-existence of both extensional and collisional tectonic settings (Partin et al., 2014). Therefore, the ca. 2.3 Ga magmatism in the Taihua Complex was related to orogenic collapse that resulted in an extensional setting along the southern TNCO, which is consistent with the global tectonic regime at this time.

6. Conclusions

The gneisses in the Taihua Complex can be subdivided into three groups based on geochronological and geochemical data. Group-1 rocks resulted from the partial melting of pre-existing TTG and K-rich rocks at high-temperature–low-pressure conditions. Group-2 rocks were generated by the high-degree partial melting of ancient crust. Group-3 rocks were formed by the partial melting of delaminated lower crust.

The gneisses in the Taihua Complex have variable whole-rock Nd—Hf and zircon Hf—O isotopic compositions, reflecting the dominance of crustal recycling along with subordinate crustal growth in the southern TNCO during the early Paleoproterozoic. The Taihua Complex records extensive magmatism at ca. 2.3 Ga, which resulted from orogenic collapse, extensional tectonics, and lithospheric delamination.

Declaration of Competing Interest

The authors declare that they have no known competing financial interests or personal relationships that could have appeared to influence the work reported in this paper.

Acknowledgement

We appreciate Q. Yang, X.P. Xia, Y.N. Yang, J.L. Ma, L. Zhang, X.R. Liang and X.L. Tu for their analytical assistance. We are grateful to two anonymous reviewers for their careful reviews and constructive comments, and thank Prof. X.L. Wang for his editorial handling of this paper. This study was financially supported by the National Natural Science Foundation of China (NSFC Projects 41625007, 41903029, 42021002, 41373032), and the Key Special Project for Introduced Talents Team of Southern Marine Science and Engineering Guangdong Laboratory (Guangzhou) (GML2019ZD0202). This is contribution No. IS-3030 from GIGCAS.

Appendix A. Supplementary data

Supplementary data to this article can be found online at https://doi.org/10.1016/j.lithos.2021.106248.

References

Aspler, L.B., Chiarenzelli, J.R., 1998. Two Neoarchean supercontinents? Evidence from the Paleoproterozoic. Sediment. Geol. 120, 75–104.

Barker, F., Arth, J.G., 1976. Generation fo trondhjemitic-tonaitic liquids and Archean bimodal trondhjemite-basalt suites. Geology 4, 596.

Bindeman, I.N., Eiler, J.M., Yogodzinski, G.M., Tatsumi, Y., Stern, C.R., Grove, T.L., Portnyagin, M., Hoernle, K., Danyushevsky, L.V., 2005. Oxygen isotope evidence for slab melting in modern and ancient subduction zones. Earth Planet. Sci. Lett. 235, 480–496.

Booth, A.L., Kolodny, Y., Chamberlain, C.P., McWiliams, M., Schmitt, A.K., Wooden, J., 2005. Oxygen isotopic composition and U-Pb discordance in zircon. Geochim. Cosmochim. Acta 69, 4895–4905.

Cawood, P.A., Hawkesworth, C.J., Dhuime, B., 2013. The continental record and the generation of continental crust. Geol. Soc. Am. Bull. 125, 14–32.

Condie, K.C., 2005. TTGs and adakites: are they both slab melts? Lithos 80, 33–44.

Condie, K.C., O'Neill, C., Aster, R.C., 2009. Evidence and implications for a widespread magmatic shutdown for 250 My on Earth. Earth Planet. Sci. Lett. 282, 294–298.

Cui, X.Z., Wang, J., Sun, Z.M., Wang, W., Deng, Q., Ren, G.M., Liao, S.Y., Huang, M.D., Chen, F.L., Ren, F., 2019. Early Paleoproterozoic (ca. 2.36 Ga) post-collisional granitoids in Yunnan, SW China: Implications for linkage between Yangtze and Laurentia in the Columbia supercontinent. J. Asian Earth Sci. 169, 308–322.

Dan, W., Li, X.H., Guo, J.H., Liu, Y., Wang, X.C., 2012. Paleoproterozoic evolution of the eastern Alxa Block, westernmost North China: evidence from in situ zircon U-Pb dating and Hf-O isotopes. Gondwana Res. 21, 838–864.
Diwu, C.R., Sun, Y., Gao, J.F., Fan, L.G., 2013. Early Precambrian tectonothermal events of the North China Craton: Constraints from in situ detrital zircon U-Pb, Hf and O isotopic compositions in Tietonggou Formation. Chin. Sci. Bull. 58, 3760–3770.
Diwu, C.R., Sun, Y., Zhao, Y., Lai, S.C., 2014. Early Paleoproterozoic (2.45–2.20 Ga) magmatic activity during the period of global magmatic shutdown: Implications for the crustal evolution of the southern North China Craton. Precambrian Res. 255, 627–640.
Dong, C.Y., Liu, D.Y., Wan, Y.S., Xu, Z.Y., Wang, W., Xie, H.Q., 2009. Hf isotope composition and REE pattern of zircons from early Precambrian metamorphic rocks in the Daqing Mountains, Inner Mongolia. Geol. Rev. 55, 509–520 (in Chinese with English abstrast).
Drummond, M.S., Defant, M.J., 1990. A model for Trondhjemite-Tonalite-Dacite genesis and crustal growth via slab melting Archean to Modern comparisons. J. Geopgysical Res. 95, 21503–21521.
Eriksson, P.G., Condie, K.C., 2014. Cratonic sedimentation regimes in the ca. 2450–2000Ma period: Relationship to a possible widespread magmatic slowdown on Earth? Gonawana Res. 25, 30–47.
Gong, S.L., Chen, N.S., Geng, H.Y., Sun, M., Zhang, L., Wang, Q.Y., 2014. Zircon Hf isotopes and geochemistry of the early paleoproterozoic high-Sr low-Y quartz-diorite in the Quanji massif, NW China: Crustal growth and tectonic implications. J. Earth Sci. 25, 74–86.
Gong, S.L., He, C., Wang, X.C., Chen, N.S., Kusky, T.M., 2019. No plate tectonic shutdown in the early Paleoproterozoic: Constraints from the ca. 2.4 Ga granitoids in the Quanji Massif, NW China. J. Asian Earth Sci. 172, 221–242.
Guan, B.D. (Ed.), 1996. The Precambrian-Lower Cambrian Geology and Metallogensis in the South Border of the North China Platform in Henan Province. Press of China University of Geoscience, Wuhan, pp. 1–328 (in Chinese).
Hawkesworth, C.J., Kemp, A.I.S., 2006. Evolution of the continental crust. Nature 443, 811–817.
He, C., Gong, S.L., Wang, L., Chen, N.S., Santosh, M., Wang, Q.Y., 2018. Protracted post-collisional magmatism during plate subduction shutdown in early Paleoproterozoic: Insights from post-collisional granitoid suite in NW China. Gondwana Res. 55, 92–111.
Huang, X.L., Wilde, S.A., Yang, Q.J., Zhong, J.W., 2012. Geochronology and petrogenesis of gray gneisses from the Taihua Complex at Xiong'er in the southern segment of the Trans-North China Orogen: Implications for tectonic transformation in the Early Paleoproterozoic. Lithos 134–135, 236–252.
Huang, X.L., Wilde, S.A., Zhong, J.W., 2013. Episodic crustal growth in the southern segment of the Trans-North China Orogen across the Archean-Proterozoic boundary. Precambrian Res. 233, 337–357.
Jia, X.L., 2016. Research for Taihua complex in Xiaoqinling and Lushan area: Implications for the evolution of the crystalline basement in southern North China Craton. Doctoral Dissertation, Xi'an. University, Northwest.
Jia, X.L., Zhu, X.Y., Zhai, M.G., Zhao, Y., Zhang, H., Wu, J.L., Liu, T., 2016. Late Mesoarchean crust growth event: evidence from the ca. 2.8Ga granodioritic gneisses of the Xiaoqinling area, southern North China Craton. Sci. Bull. 61, 974–990.
Jia, X.L., Zhai, M.G., Xiao, W.J., Sun, Y., Ratheesh-Kumar, R.T., Yang, H., Zhou, K.F., Wu, J.L., 2019. Late Neoarchean to early Paleoproterozoic tectonic evolution of the southern North China Craton: evidence from geochemistry, zircon geochronology and Hf isotopes of felsic gneisses from the Taihua complex. Precambrian Res. 326, 222–239.
Johnson, T.E., Brown, M., Kaus, B.J.P., Van Tongeren, J.A., 2013. Delamination and recycling of Archaean crust caused by gravitational instabilities. Nat. Geosci. 7, 47–52.
Johnson, T.E., Brown, M., Gardiner, N.J., Kirkland, C.L., Smithies, R.H., 2017. Earth's first stable continents did not form by subduction. Nature 543, 239–242.
Laurent, O., Martin, H., Moyen, J.F., Doucelance, R., 2014. The diversity and evolution of late-Archean granitoids: evidence for the onset of "modern-style" plate tectonics between 3.0 and 2.5Ga. Lithos 205, 208–235.
Li, S.Z., Zhao, G.C., 2007. SHRIMP U-Pb zircon geochronology of the Liaoji granitoids: Constraints on the evolution of the Paleoproterozoic Jiao-Liao-Ji belt in the Eastern Block of the North China Craton. Precambrian Res. 158, 1–16.
Li, X.H., Tang, G.Q., Gong, B., Yang, Y.H., Hou, K.J., Hu, Z.C., Li, Q.L., Liu, Y., Li, W.X., 2013. Qinghu zircon: a working reference for microbeam analysis of U-Pb age and Hf and O isotopes. Chin. Sci. Bull. 58, 4647–4654.
Liu, D.Y., Nutman, A.P., Compston, W., Wu, J.S., Shen, Q.H., 1992. Remnants of ≥3800 Ma crust in the Chinese part of the Sino-Korean craton. Geology 20, 339–342.
Liu, D.Y., Wilde, S.A., Wan, Y.S., Wang, S.Y., Valley, J.W., Kita, N., Dong, C.Y., Xie, H.Q., Yang, C.X., Zhang, Y.X., Gao, L.Z., 2009. Combined U-Pb, hafnium and oxygen isotope analysis of zircons from meta-igneous rocks in the southern North China Craton reveal multiple events in the Late Mesoarchean-Early Neoarchean. Chem. Geol. 261, 140–154.
Ludwig, K.R., 2003. User's manual for ISOPLOT 3.00: a geochronological toolkit for microsoft excel. Berkeley Geochronology Center Special Publication 4 pp. 1–67.
Lustrino, M., 2005. How the delamination and detachment of lower crust can influence basaltic magmatism. Earth Sci. Rev. 72, 21–38.
Ma, Q., Xu, Y.G., Huang, X.L., Zheng, J.P., Ping, X.Q., Xia, X.P., 2020. Eoarchean to Paleoproterozoic crustal evolution in the North China Craton: evidence from U-Pb and Hf-O isotopes of zircons from deep-crustal xenoliths. Geochim. Cosmochim. Acta 278, 94–109.
Martin, H., Smithies, R.H., Rapp, R., Moyen, J.F., Champion, D., 2005. An overview of adakite, tonalite-trondhjemite-granodiorite (TTG), and sanukitoid: relationships and some implications for crustal evolution. Lithos 79, 1–24.
Moyen, J.F., 2009. High Sr/Y and La/Yb ratios: the meaning of the "adakitic signature". Lithos 112, 556–574.
Moyen, J.F., Martin, H., 2012. Forty years of TTG research. Lithos 148, 312–336.
Müller, D., Groves, D.I. (Eds.), 1997. Potassic Igneous Rocks and Associated Gold-Copper Mineralization. Springer-Verlag, Berlin Heidelberg, pp. 1–225.
Nelson, D.R., 1992. Isotopic characteristics of potassic rocks: evidence for the involvement of subducted sediments in magma genesis. Lithos 28, 403–420.
Partin, C.A., Bekker, A., Sylvester, P.J., Wodicka, N., Stern, R.A., Chacko, T., Heaman, L.M., 2014. Filling in the juvenile magmatic gap: evidence for uninterrupted Paleoproterozoic plate tectonics. Earth Planet. Sci. Lett. 388, 123–133.
Qi, J.Y., 1992. Metamorphic rock series of Taihua Group and conditions for its formation in eastern Qinling. Sci. Geol. Sin. 27, 94–107 (in Chinese with English abstract).
Qian, Q., Hermann, J., 2013. Partial melting of lower crust at 10–15 kbar: constraints on adakite and TTG formation. Contrib. Mineral. Petrol. 165, 1195–1224.
Rapp, R.P., Shimizu, N., Norman, M.D., Applegate, G.S., 1999. Reaction between slab-derived melts and peridotite in the mantle wedge: experimental constraints at 3.8 GPa. Chem. Geol. 160, 335–356.
Seixas, L.A.R., David, J., Stevenson, R., 2012. Geochemistry, Nd isotopes and U-Pb geochronology of a 2350Ma TTG suite, Minas Gerais, Brazil: Implications for the crustal evolution of the southern São Francisco craton. Precambrian Res. 196–197, 61–80.
Shen, F.N., 1986. Discussion on the relational questions of Taihua Group in Minor Qinling Range. J. Northwest University 16, 43–51 (in Chinese with English abstract).
Sláma, J., Košler, J., Condon, D.J., Crowley, J.L., Gerdes, A., Hanchar, J.M., Horstwood, M.S.A., Morris, G.A., Nasdala, L., Norberg, N., Schaltegger, U., Schoene, B., Tubrett, M.N., Whitehose, M.J., 2008. Plešovice zircon—A new natural reference material for U–Pb and Hf isotopic microanalysis. Chem. Geol. 249, 1–35.
Smithies, R.H., Champion, D.C., 2000. The Archaean High-Mg Diorite Suite: Links to Tonalite-Trondhjemite-Granodiorite Magmatism and Implications for early Archaean Crustal Growth. J. Petrol. 41, 1653–1671.
Song, B., Nutman, A.P., Liu, D.Y., Wu, J.S., 1996. 3800 to 2500 Ma crustal evolution in the Anshan area of Liaoning Province, northeastern China. Precambrian Res. 78, 79–94.
Spencer, C.J., Murphy, J.B., Kirkland, C.L., Liu, Y.B., Mitchell, R.N., 2018. A Palaeoproterozoic tectono-magmatic lull as a potential trigger for the supercontinent cycle. Nat. Geosci. 11, 97–101.
Sun, S.S., McDonough, W.F., 1989. Chemical and isotopic systematics of oceanic basalts: implications for mantle composition and processes. Geol. Soc. Lond., Spec. Publ. 42, 313–345.
Tam, P.Y., Zhao, G., Liu, F., Zhou, X., Sun, M., Li, S., 2011. Timing of metamorphism in the Paleoproterozoic Jiao-Jiao-Ji Belt: New SHRIMP U-Pb zircon dating of granulites, gneisses and marbles of the Jiaobei massif in the North China Craton. Gondwana Res. 19, 150–162.
Tchameni, R., Mezger, K., Nsifa, E.N., Pouclet, A., 2001. Crustal origin of Early Proterozoic syenites in the Congo Craton (Ntem Complex), South Cameroon. Lithos 57, 23–42.
Teixeira, W., Ávila, C.A., Dussin, I.A., Corrêa Neto, A.V., Bongiolo, E.M., Santos, J.O., Barbosa, N.S., 2015. A juvenile accretion episode (2.35–2.32Ga) in the Mineiro belt and its role to the Minas accretionary orogeny: Zircon U-Pb-Hf and geochemical evidences. Precambrian Res. 256, 148–169.
Trap, P., Faure, M., Lin, W., Monié, P., 2007. Late Paleoproterozoic (1900–1800Ma) nappe stacking and polyphase deformation in the Hengshan-Wutaishan area: Implications for the understanding of the Trans-North-China Belt, North China Craton. Precambrian Res. 156, 85–106.
Valley, J.W., Kinny, P.D., Schulze, D.J., Spicuzza, M.J., 1998. Zircon megacrysts from kimberlite: oxygen isotope variability among mantle melts. Contrib. Mineral. Petrol. 133, 1–11.
Valley, J.W., Lackey, J.S., Cavosie, A.J., Clechenko, C.C., Spicuzza, M.J., Basei, M.A.S., Bindeman, I.N., Ferreira, A.N., Sial, A.N., King, E.M., Peck, W.H., Sinha, A.K., Wei, C.S., 2005. 4.4 billion years of crustal maturation: oxygen isotope ratios of magmatic zircon. Contrib. Mineral. Petrol. 150, 561–580.
Vervoort, J.D., Plank, T., Prytulak, J., 2011. The Hf-Nd isotopic composition of marine sediments. Geochim. Cosmochim. Acta 75, 5903–5926.
Wang, Q., Xu, J.F., Jian, P., Bao, Z.W., Zhao, Z.H., Li, C.F., Xiong, X.L., Ma, J.L., 2006. Petrogenesis of adakitic porphyries in an extensional tectonic setting, Dexing, South China: Implications for the genesis of porphyry copper mineralization. J. Petrol. 47, 119–144.
Wang, G.D., Wang, H., Chen, H.X., Lu, J.S., Xiao, L.L., Wu, C.M., 2012. U-Pb dating of zircons from metamorphic rocks of the Taihua Metamorphic complex, Mt. Huashan, southern margin of the Trans-North China Orogen. Acta Geol. Sin. 86, 1541–1551 (in Chinese with English abstract).
Wang, G.D., Wang, H., Chen, H.X., Lu, J.S., Wu, C.M., 2014. Metamorphic evolution and zircon U-Pb geochronology of the Mts. Huashan amphibolites: Insights into the Palaeoproterozoic amalgamation of the North China Craton. Precambrian Res. 245, 100–114.
Wang, G.D., Wang, H.Y.C., Chen, H.X., Zhang, B., Zhang, Q., Wu, C.M., 2017a. Geochronology and geochemistry of the TTG and potassic granite of the Taihua complex, Mts. Huashan: Implications for crustal evolution of the southern North China Craton. Precambrian Res. 288, 72–90.
Wang, X., Huang, X.L., Yang, F., Luo, Z.X., 2017b. Late Neoarchean magmatism and tectonic evolution recorded in the Dengfeng complex in the southern segment of the Trans-North China Orogen. Precambrian Res. 302, 180–197.
Wang, X., Huang, X.L., Yang, F., 2019. Revisiting the Lushan-Taihua complex: New perspectives on the late Mesoarchean-early Neoarchean crustal evolution of the southern North China Craton. Precambrian Res. 325, 132–149.
Watkins, J.M., Clemens, J.D., Treloar, P.J., 2007. Archaean TTGs as sources of younger granitic magmas: melting of sodic metatonalites at 0.6–1.2 GPa. Contrib. Mineral. Petrol. 154, 91–110.
Wei, C.S., Zheng, Y.F., Zhao, Z.F., Valley, J.W., 2002. Oxygen and neodymium isotope evidence for recycling of juvenile crust in Northeast China. Geology 30, 375–378.
Wu, F.Y., Li, X.H., Zheng, Y.F., Gao, S., 2007. Lu-Hf isotopic systematics and their applications in petrology. Acta Petrol. Sin. 23, 185–220 (in Chinese with English abstract).

Xiong, X.L., 2006. Trace element evidence for growth of early continental crust by melting of rutile-bearing hydrous eclogite. Geology 34, 945.
Xiong, X.L., Adam, J., Green, T.H., 2005. Rutile stability and rutile/melt HFSE partitioning during partial melting of hydrous basalt: Implications for TTG genesis. Chem. Geol. 218, 339–359.
Yang, Q., Xia, X., Zhang, W., Zhang, Y., Xiong, B., Xu, Y., Wang, Q., Wei, G., 2018. An evaluation of precision and accuracy of SIMS oxygen isotope analysis. Solid Earth Sciences 3, 81–86.
Yu, X.Q., Liu, J.L., Li, C.L., Chen, S.Q., Dai, Y.P., 2013. Zircon U-Pb dating and Hf isotope analysis on the Taihua complex: Constraints on the formation and evolution of the Trans-North China Orogen. Precambrian Res. 230, 31–44.
Yu, X.J., Fu, S.T., Wang, Z.D., Li, Q., Guo, Z.J., 2017. The discovery of early Paleoproterozoic high-Na trondhjemite in the northeastern Qaidam basin: evidence from the drilling core samples. Precambrian Res. 298, 615–628.
Yuan, L.L., Zhang, X.H., Yang, Z.L., Lu, Y.H., Chen, H.H., 2017. Paleoproterozoic Alaskan-type ultramafic-mafic intrusions in the Zhongtiao mountain region, North China Craton: Petrogenesis and tectonic implications. Precambrian Res. 296, 39–61.
Zhai, M.G., Liu, W.J., 2003. Palaeoproterozoic tectonic history of the North China Craton: a review. Precambrian Res. 122, 183–199.
Zhang, C.L., Li, Z.X., Li, X.H., Yu, H.F., Ye, H.M., 2007. An early Paleoproterozoic high-K intrusive complex in southwestern Tarim Block, NW China: Age, geochemistry, and tectonic implications. Gondwana Res. 12, 101–112.
Zhang, L., Ren, Z.Y., Xia, X.P., Li, J., Zhang, Z.F., 2015. IsotopeMaker: a Matlab program for isotopic data reduction. Int. J. Mass Spectrom. 392, 118–124.
Zhao, G.C., Zhai, M.G., 2013. Lithotectonic elements of Precambrian basement in the North China Craton: Review and tectonic implications. Gondwana Res. 23, 1207–1240.
Zhao, G.C., Sun, M., Wilde, S.A., Li, S.Z., 2005. Late Archean to Paleoproterozoic evolution of the North China Craton: key issues revisited. Precambrian Res. 136, 177–202.
Zhao, G.C., Wilde, S.A., Sun, M., Li, S.Z., Li, X.P., Zhang, J., 2008. SHRIMP U-Pb zircon ages of granitoid rocks in the Lüliang Complex: Implications for the accretion and evolution of the Trans-North China Orogen. Precambrian Res. 160, 213–226.